Science and Technology Indonesia
e-ISSN:2580-4391 *p*-ISSN:2580-4405
Vol. 11, No. 3, July 2026

Research Paper

Unravelling the Potential of Wild Endemic Sumatran Turmeric (*Curcuma sumatrana* Miq.) as a Candidate of Herbal Medicine for Neurodegenerative Diseases

Putra Santoso[1*], Syafruddin Ilyas[2], Rita Maliza[1], Indah Fajarwati[3], Rauza Sukma Rita[4], Aldi Tamara Rahman[1], Jihan Aprilia Nawawi[1], Ivan Petrovsky[1], Muhammad Samudra Ilham[1], Ananda Fitriana[1]

[1]*Department of Biology, Faculty of Mathematics and Natural Sciences, Universitas Andalas, Kampus UNAND Limau Manis Pauh, Padang, West Sumatra, 25163, Indonesia*
[2]*Department of Biology, Faculty of Mathematics and Natural Sciences, Universitas Sumatera Utara, Medan, North Sumatra, 20155, Indonesia*
[3]*Biomedical Research Center, Research Organization for Health, National Research and Innovation Agency (BRIN), Cibinong, West Java, 16911, Indonesia*
[4]*Department of Biochemistry, Faculty of Medicine, Universitas Andalas, Kampus UNAND Limau Manis Pauh, Padang, West Sumatra, 25163, Indonesia*
*__Corresponding author__: putrasantoso@sci.unand.ac.id

Abstract
Neurodegenerative diseases pose significant health challenges, while synthetic drugs are often associated with detrimental side effects. Hence, the search for herbal medicines is warranted. *Curcuma sumatrana* is traditionally used by Minangkabau people as a herbal medicine, but it remains scientifically underexplored. This study aims to evaluate its neuroprotective potential through phytochemical profiling, computational analyses, and biological assays. LC-MS/MS-QTOF profiling identified 13 compounds in the rhizome extract, predominantly terpenoids. *In silico* analyses predicted antioxidant, anti-inflammatory, and antineurodegenerative activities, while drug-likeness assessment suggested favorable bioavailability for all identified compounds. Furthermore, molecular docking targeting neurodegeneration-associated proteins revealed strong interactions of compounds namely brefeldin A, nigakilactone K, genistein, and 8-epi-loganic acid-6'-O-β-D-glucoside with MAPK1, TNF-α, BACE1, and CASP3, respectively. In addition, the extract exhibited notable antioxidant activity in the DPPH assay and ameliorated monosodium glutamate-induced cognitive impairment, hippocampal neurodegeneration, and elevated brain malondialdehyde levels in mice. Hence, *C. sumatrana* is a promising herbal medicine for neurodegenerative diseases, plausibly acting through the modulation of neurodegeneration-related pathways and antioxidant mechanisms. These findings provide a foundation for future drug discovery by identifying bioactive compounds with potential applications in the management of neurodegenerative disorders.

Keywords
Antioxidant, Cognitive Deficits, *Curcuma sumatrana*, Hippocampus, Malondialdehyde

Received: 26 March 2026, Accepted: 17 June 2026
https://doi.org/10.26554/sti.2026.11.3.1212-1240

1. INTRODUCTION

Neurodegenerative diseases, such as Alzheimer's and Parkinson's, represent critical global health burdens, exacerbated by aging populations and limited therapeutic options (Wang et al., 2024). Current treatments for neurodegeneration often target symptoms rather than underlying mechanisms (Passeri et al., 2022), while synthetic drugs are expensive and reported to cause various detrimental side effects (Fan et al., 2022). Hence, it is necessary to explore the safer, affordable and multi-targeted alternative medicines including herbal medicines. Natural products, particularly those rich in antioxidant and anti-inflammatory phytochemicals, have emerged as promising candidates due to their ability to modulate oxidative pathways and neuroinflammatory cascades (Sarkar et al., 2024). Among these, turmeric species (*Curcuma* spp.; Zingiberaceae) are renowned for their medicinal properties in managing neurodegeneration (Sohrab et al., 2024; Genchi et al., 2024; Pomalango et al., 2025). A previous report demonstrated that *C. kawangsinensis* extract exerts notable antioxidant effect due to its bioactive compounds in the group of diarylheptanoids (Chen et al., 2022). An *in vitro* study also reported that sesquiterpenoids from *C. aromatica* could enhance endogenous antioxidant enzymes including superoxide dismutase, catalase, and glutathione superoxide dismutase (Dai et al., 2023). Another *in vitro* and *in vivo* experiment revealed the neuroprotective potential of *C. longa* extract in alleviating corticosterone-induced neurotoxicity (Oh et al., 2025). The protective effect of *C. longa* is attributed to high level of curcuminoids content in the rhizome (Shahrajabian and Sun, 2024). Furthermore, an experiment conducted by Qi et al. (2025) demonstrated that the ethyl acetate extract of *C. wenyujin* effectively counteracts

Alzheimer's disease by inhibiting pyroptosis while promoting mitophagy and suppressing neuroinflammatory responses in mice model. Collectively, these findings clearly indicate the potential of medicinal plants in the genus of *Curcuma* as alternative medicines in counteracting neurodegenerative diseases.

Konih rimbo (*C. sumatrana* Miq.) is one of prospective candidates of alternative medicines from the genus of *Curcuma*. This wild species is endemic to Sumatra Island, widely distributed in the rain forest areas of West Sumatra (Syafira et al., 2024). The leaves and rhizomes of *C. sumatrana* have been traditionally used by the Minangkabaunese as an ethnomedicine to heal gastrointestinal diseases and skin infection (Syafira et al., 2024; Yuhendri et al., 2024). Recently, this species gains more scientific attentions in term of its medicinal benefits. A previous report has demonstrated antimicrobial activity of *C. sumatrana* extract against *Staphylococcus aureus* (Alamsjah et al., 2023) while *in silico* simulations suggest its anticancer potential (Rahman et al., 2022). Our previous study also revealed that *C. sumatrana* ethanolic extract exerts its therapeutic effect in mice suffering from non-alcoholic fatty liver disease (Santoso et al., 2024). Moreover, another *in silico* simulation suggests the potential of some bioactive compounds from *C. sumatrana* in activating endogenous antioxidant proteins including catalase, superoxide dismutase and Kelch-like ECH-associated protein 1 (Keap1) (Petrovsky et al., 2026). However, no studies have so far investigated its actual antioxidant activities for both *in vitro* and *in vivo*. Moreover, scientific evidence for its anti-neurodegenerative activities also remains limited.

In the complex pathogenesis of neurodegenerative diseases, proteins such as mitogen-activated protein kinase 1 (MAPK1), beta-site APP cleaving enzyme 1 (BACE1), tumor necrosis factor alpha (TNF-α), and caspase-3 (CASP3) play critical roles. These signalling proteins are simultaneously integrated in pathological pathways as follows. Activation of MAPK1 contributes to microglial activation, reactive oxygen species (ROS) generation, mitochondrial dysfunction, and increases the expression of TNF-α (Wu et al., 2025; Jeon et al., 2025). Furthermore, activation of MAPK1 and TNF-α pathways upregulates BACE1 expression, thereby connecting neuroinflammation with amyloidogenesis (Bartolić and Bosak, 2025). Subsequently, the increased BACE1 activity activates CASP3-mediated neuronal cell death (Shi et al., 2026). In addition, MAPK1 and TNF-α signaling pathways can also directly promote caspase-3 activation (Wójcik et al., 2024). It has been shown that TNF-α creates a neurotoxic environment that exacerbates neuronal damage in neurodegenerative disorders such as Alzheimer's disease and Parkinson's disease (Andronie-Cioara et al., 2023). In addition, dysregulation of MAPK1 contributes to neuroinflammation, synaptic dysfunction, and neuronal death (Wu et al., 2025), whereas BACE1 plays a central role in the generation of neurotoxic amyloid-β peptides that accumulate as plaques and drive the progression of Alzheimer's disease pathology (Bi et al., 2025). CASP3 acts as a key executioner protease involved in apoptotic neuronal loss during neurodegeneration (Wójcik et al., 2024). Therefore, inhibition of MAPK1, TNF-α, BACE1, and CASP3 may provide targeted control over the development and progression of neurodegenerative diseases. However, to our knowledge, until recently, there is no information regarding the potential of bioactive compounds from *C. sumatrana* in inhibiting the activities of these proteins.

In a study of neurodegenerative diseases, animal models could be developed using chemical, genetic, surgical, metabolic, or aging-related approaches to mimic neuronal degeneration, oxidative stress, neuroinflammation, and cognitive impairment observed in human disorders (Mishra and Upadhyay, 2025). One of chemicals used to induce neurodegeneration is monosodium glutamate (MSG). MSG is well documented to induce excitotoxicity through excessive glutamatergic stimulation, leading to increased ROS production, mitochondrial dysfunction, and neuroinflammation (Essawy et al., 2025). These mechanisms are strongly associated with key pathological features observed in neurodegenerative disorders, including Alzheimer's disease. Although this model does not fully recapitulate the complete complexity of Alzheimer's pathology (amyloid-beta plaque formation and tau hyperphosphorylation), it is widely used as an experimental model to study oxidative stress-mediated neurodegeneration and cognitive impairment (Khalil and Khedr, 2016; Essawy et al., 2025).

In the context of neurodegenerative diseases, several species of the genus *Curcuma* have been widely studied for their therapeutic potential (Pomalango et al., 2025; Perez et al., 2025); however, research on *C. sumatrana* is still very limited. Previous studies mainly focused on preliminary phytochemical screening, which only confirmed the presence of major secondary metabolite groups (Alamsjah et al., 2023), without identifying the specific compounds responsible for the biological activities. In addition, earlier investigations generally emphasized antioxidant activity by *in silico* simulation (Petrovsky et al., 2026) and did not explore the possible underlying mechanisms related to neurodegenerative diseases. To date, no study has comprehensively examined the neuroprotective potential of *C. sumatrana* by combining detailed metabolite identification, molecular interaction prediction, and biological validation in animal models. Therefore, the present study deploys an integrative approach by combining LC–MS/MS QTOF-based phytochemical profiling to specifically identify alkaloid, flavonoid, and terpenoid compounds, together with *in silico* molecular docking analysis against neurodegeneration-related proteins, including MAPK1, TNF-α, BACE1, and CASP3. The study also evaluates the antioxidant activity of the extract using three different assays (DPPH, ABTS, and FRAP) and further validates its neuroprotective effects through MSG-induced neurodegenerative mouse model. This study aims to elucidate the neuroprotective potential of *C. sumatrana* and new mechanistic insights into its possible role as a natural therapeutic candidate for neurodegenerative disorders.

2. EXPERIMENTAL SECTION

2.1 Materials

Materials used in this study were ethanol, formic acid, acetonitrile, 2,2-Diphenyl-1-picrylhydrazyl (DPPH), ascorbic acid, trolox, ferric reducing antioxidant power (FRAP) reagent, 2,2'-Azino-bis (3-ethylbenzothiazoline-6-sulfonic acid) (ABTS), potassium persulfate, monosodium glutamate, phosphate-buffered saline, neutral buffered formalin, xylene, paraffin paraplast, hematoxylin-eosin staining kit (Sigma-Aldrich, USA), lipid peroxidation assay kit (Abcam, USA), Ratbio (Citra Inna Feed, Indonesia), and adult male BALB/c mice (Balai Veteriener Baso).

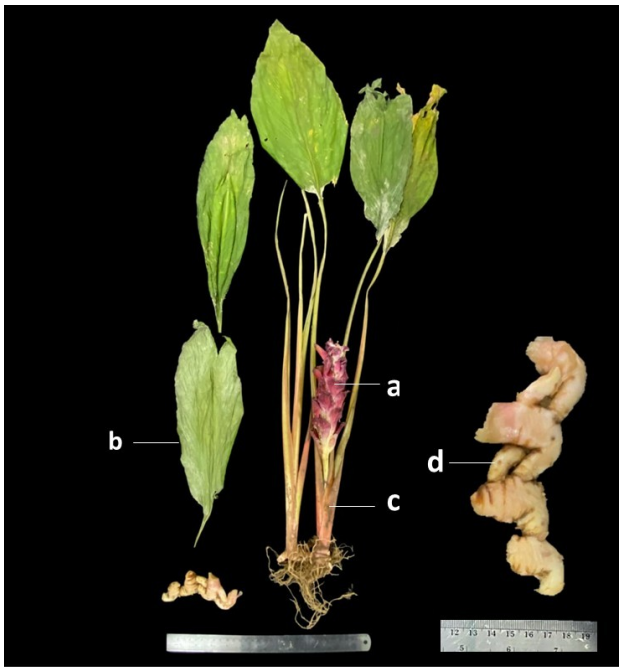

Figure 1. Photograph of *C. sumatrana* Specimen. (a) Flower, (b) Leaf, (c) Stem, (d) Rhizome

2.2 Methods

2.2.1 Sample Collection and Extraction

Fresh rhizomes of *C. sumatrana* (5 kg of wet weight) were collected from a forest area in Koto Pulai, Lengayang Pesisir Selatan, West Sumatra (geographical coordinates: 1°35'58.2"S, 100°50'31.0"E). The species was taxonomically authenticated by Dr. Nurainas at Herbarium ANDA of Universitas Andalas (Voucher specimen No. 00049122; Authentication document No. 543/K-ID/ANDA/XI/22; Figure 1). The rhizome samples were rinsed thoroughly with tap water followed by distilled water, sliced into smaller pieces, and dried at 50 °C in a dehydrator (FDH-6 Food Dehydrator, WIRASTAR, Indonesia) until a constant weight was achieved. The dried material was then pulverized using an electric grinder (P21-Philips, Indonesia) and subjected to maceration in 96% ethanol within a light-protected bottle for three days, with daily agitation. The resulting extract was filtered through filter paper, and the residual plant material underwent additional filtrations. Finally, the combined filtrate was concentrated using a rotary evaporator (IKA RV3-V, Thermo Fisher Scientific, USA) at 60 °C under reduced pressure for 12 h (Wu et al., 2024).

2.3 Targeted Phytochemical Analysis Using LC-MS/MS-QTOF

Phytochemical screening was performed to specifically target compounds in the groups of alkaloids, terpenoids and flavonoids in the *C. sumatrana* ethanolic extract. In this analysis, biotin was used as a standard compound. The instrument used was Xevo G3 QTof (WATERS, USA). A gram of extract was diluted in ethanol and subsequently ultrasonicated for 30 min. Homogenized sample was then filtered using a General Hydrophilic Polypropylene/Polytetrafluoroethylene (GHP/PTFE) membrane filter (mesh 0.22 μm). Furthermore, 1 μL sample was injected into UPLC (ultraperformance liquid chromatography) system. The instrument of LC-MS/MS-QTOF was set with details as follows: LC instrument column C18, column temperature 400 °C, autosampler temperature 150 °C, injection volume 1 μL, mobile phase. A compossed of 0.1% formic acid in acetonitrile, mobile phase B 0.1% formic acid in double distilled water, and flow rate 0.6 mL/min. The MS setting was as follow: mode of operation Tof MSE, ionization ESI (-)/ESI (+), acquisition range 50-1200 Dalton (Oliveira et al., 2020). The data were analyzed using UNIFI software from WATERS (USA).

Compound identification was confirmed using validation criteria comprised: (1) mass accuracy with a mass error ≤ 5 ppm, reflecting a low deviation between measured and theoretical molecular masses; (2) isotopic pattern conformity assessed through isotope match M/Z RMS ppm ≤ 6 ppm and isotope match M/Z RMS (%) ≤ 10%, demonstrating agreement between experimental and theoretical isotopic profiles; (3) signal quality indicated by intensity/response values ≥ 300 to ensure sufficient peak sensitivity and reduce background noise interference; and (4) fragment ion verification requiring at least one corresponding mass fragment between the experimental MS/MS spectrum and the reference database or predicted fragmentation profile. Compounds meeting all validation requirements were regarded as confidently identified (Oliveira et al., 2020).

2.4 Evaluation of Compound Bioactivity via PASS Online Prediction

The pharmacological potential of compounds derived from *C. sumatrana* extract was investigated using the Prediction of Activity Spectra for Substances (PASS) tool, accessible through the Way2Drug platform (http://way2drug.com/PassOnline/). Initially, compound names were entered into the PubChem database (http://pubchem.ncbi.nlm.nih.gov) to retrieve their corresponding SMILES (Simplified Molecular Input Line

Table 1. Ligands and Their Respective CID and SMILES Prepared for Molecular Docking

Name	CID	SMILES
Fawcettimine	442475	C[C@@H]1C[C@H]2CC(=O)[C@@H]3 [C@]24CCCN([C@@H]4(C1)O)CCC3
Guanine	135398634	C1=NC2=C(N1)C(=O)NC(=N2)N
Genistein	5280961	C1=CC(=CC=C1C2=COC3=CC(=CC(=C3C2=O)O)O)O
Artemisic acid	10922465	C[C@@H]1CC[C@H]([C@@H]2[C@H]1CCC (=C2)C(=C)C)C(=O)O
Brefeldin A	5287620	C[C@H]1CCC/C=C/[C@@H]2[C@@H](C[C@H]2 [C@@H](/C=C/C(=O)O1)O)O
Furanodiene	9601230	C/C/1=C\CC2=C(C/C(=C\CC1)/C)OC=C2
Alpha-khusinol	91753232	CC1=C[C@H]2[C@@H](CC=C([C@@H]2 [C@H](C1)O)C)C(C)C
Linderazulene	656393	CC1=C2C=C3C(=COC3=CC(=C2C=C1)C)C
8-Epi-loganic acid-6'-O-beta-D-glucoside	163003828	CC1C(CC2C1C(OC=C2C(=O)O)OC3C(C(C(C (O3)COC4C(C(C(C(O4)CO)O)O)O)O)O)O)O
Pterosin Y	46848574	O[C@H]1[C@@@](C(=O)c2c1cc(c(c2C)CCO)CO)(CO)C
Dendronobilin F	101460596	O1[C@H]2[C@@H](O)[C@@H]3[C@H]([C@@H]3 (CO)CC[C@H]4[C@@H](C2)C1=O)CO
Nigakilactone K	12313357	C[C@@H]1C=C(C(=O)[C@]2([C@H]1C[C@@H]3 [C@@]4([C@@H]2[C@H]([C@H]([C@@H] (C4=CC(=O)O3)(C)O)OC)O)C)C)OC
Picrasin G	182244	C[C@@H]1C[C@H](C(=O)[C@]2([C@H]1C[C@@H]3 [C@@]4([C@@H]2C(=O)C(=C([C@@H]4 (CC(=O)O3)(C)OC)C)C)O)C)O
7-[2-(Oxan-4-Ylamino)pyrimidin-4-Yl]-3,4-dihydro-2-{h}-Pyrrolo[1,2-A]pyrazin-1-One (standard drug as MAPK1 inhibitor)	126480566	C1COCCC1NC2=NC=CC(=N2)C3=CN4 CCNC(=O)C4=C3
6,7-dimethyl-3-[(methyl{2-[methyl({1-[3-(trifluoromethyl)phenyl]-1h-indol-3-yl}methyl)amino]ethyl}amino)methyl]-4h-chromen-4-one (standard drug as TNF-α inhibitor)	5327044	CC1=CC2=C(C=C1C)OC=C(C2=O)CN(C) CCN(C)CC3=CN(C4=CC=CC=C4)C5=CC =CC(=C5)C(F)(F)F
(2E)-2-imino-3-methyl-5,5-diphenylimidazolidin-4-one (standard drug as BACE1 inhibitor)	15054176	CN1C(=O)C(NC1=N)(C2CCCCC2)C3CCCCC3
Benzyloxycarbonyl-Asp-Glu-Val-Asp-fluoromethylketone (standard drug as CASP3 inhibitor)	9830615	COC(=O)CC[C@H](NC(=O)[C@H](CCC(=O)OC) NC(=O)[C@H](C(C)C)NC(=O)[C@H] (CC(=O)OC)C(=O)CF)C(=O)OCC1=CC=CC=C1

Entry System) structural notations. These SMILES data were then input into the Way2Drug server to generate predictions of their biological activities. Activity probabilities (Pa values) were categorized as follows: (i) Pa > 0.7: high likelihood of biological activity; (ii) 0.5 < Pa ≤ 0.7: moderate likelihood; (iii) Pa ≤ 0.5: low probability of significant activity (Alam et al., 2021).

2.5 Assessment of Drug-Likeness via Lipinski's Rule of Five

The drug-like properties of the compounds were analyzed in accordance with Lipinski's pharmacokinetic guidelines. Canonical SMILES notations of the compounds were input into the Molinspiration Cheminformatics platform (https://www.molinspiration.com/cgi/properties) to evaluate their adherence to Lipinski's criteria. This computational tool calculated key parameters (e.g., molecular weight, logP, hydrogen bond donors/acceptors) to predict oral bioavailability and drug-

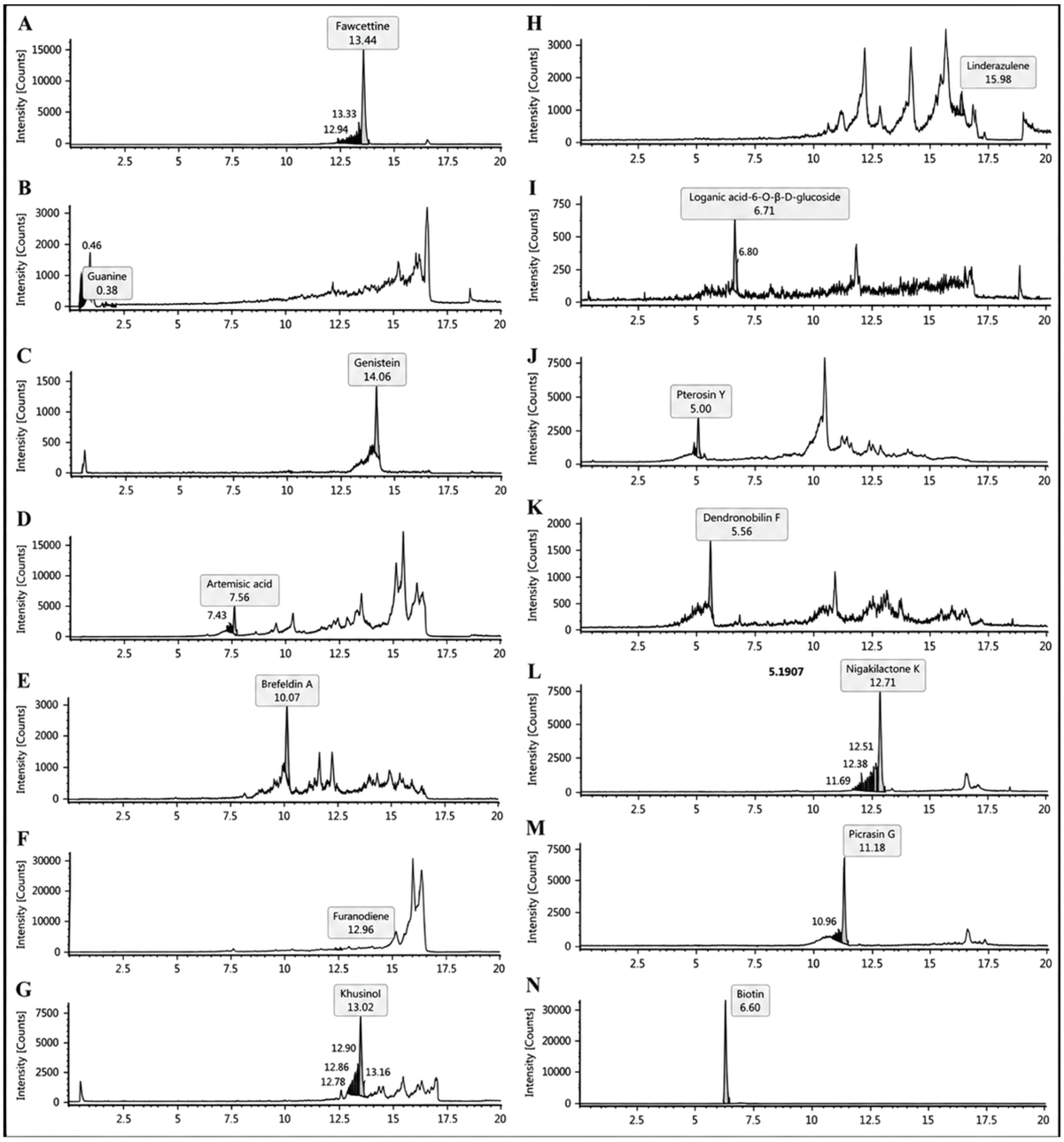

Figure 2. Chromatogram of Selective Compounds of *C. sumatrana* Extract (ECS) Based on LC-MS/MS-QTOF Elucidation. (A) Fawcettimine, (B) Guanine, (C) Genistein, (D) Artemisic acid, (E) Brefeldin A, (F) Furanodiene, (G) Alpha-khusinol, (H) Linderazulene, (I) Loganic acid-6'-O-beta-D-glucoside, (J) Pterosin Y, (K) Dendronobilin F, (L) Nigakilactone K, (M) Picrasin G, (N) Biotin as a Standard Compound

likeness (Chen et al., 2020).

2.6 Pharmacokinetic and Toxicity Profiling of Phytochemical Compounds

The ADMET (absorption, distribution, metabolism and toxicity) profile of the compounds were predicted through computational tools. First, 2D molecular structures in .sdf format and SMILES notations were retrieved from the PubChem Database (https://pubchem.ncbi.nlm.nih.gov). ADME parameters were subsequently analyzed using the SwissADME platform (http://www.swissadme.ch). Toxicity profiles were evaluated using the ProTox-II tool (http://tox-new.charite.de/protox_II), with toxicity classifications aligned to OECD (Organisation for Economic Co-operation and Development)

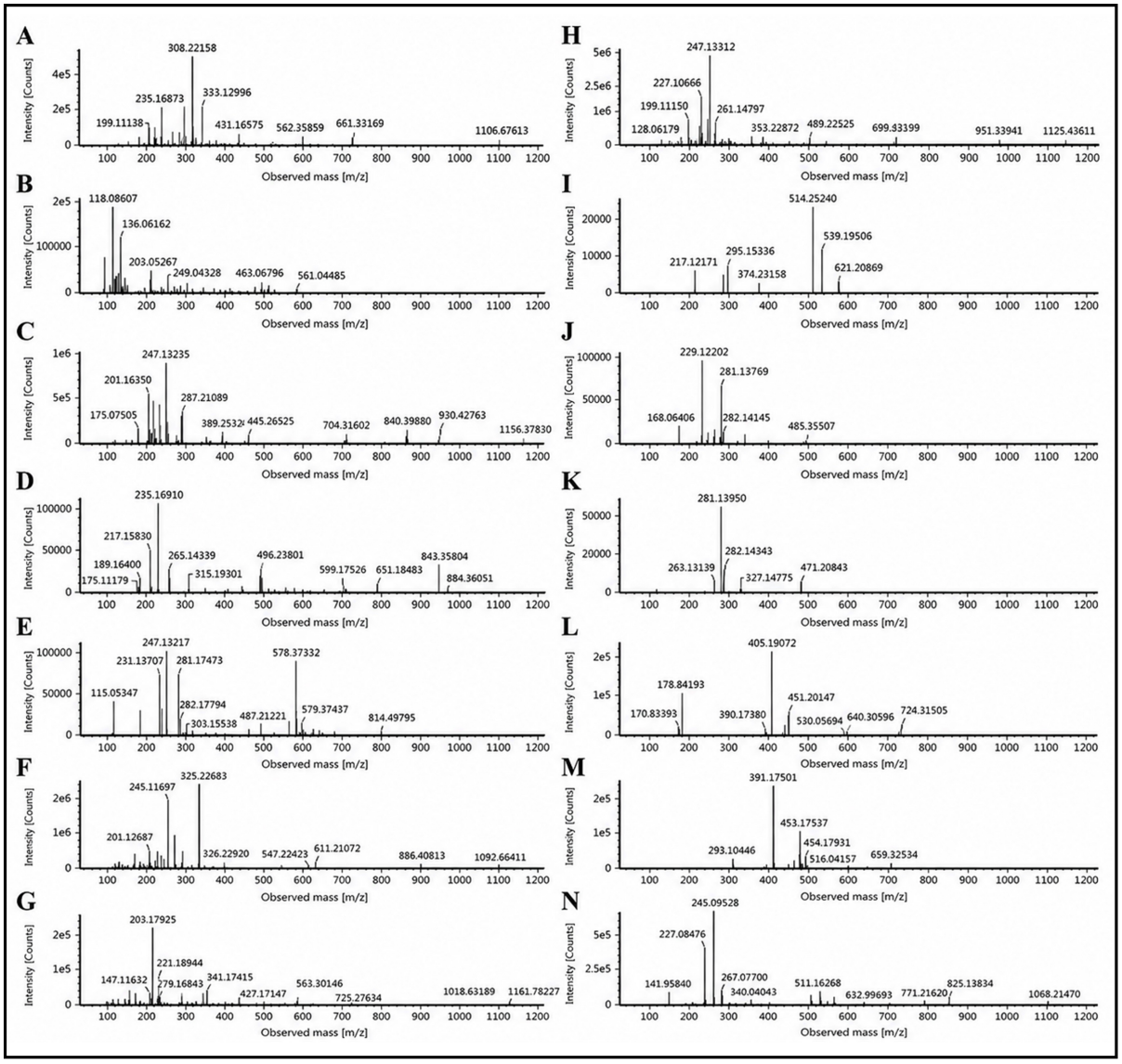

Figure 3. Fragmentation Spectra of the Selective Compounds of *C. sumatrana* Extract Based on LC-MS/MS-QTOF Analysis. (A) Fawcettimine, (B) Guanine, (C) Genistein, (D) Artemisic acid, (E) Brefeldin A, (F) Furanodiene, (G) Alpha-khusinol, (H) Linderazulene, (I) Loganic acid-6'-O-beta-D-glucoside, (J) Pterosin Y, (K) Dendronobilin F, (L) Nigakilactone K, (M) Picrasin G, (N) Biotin as a Standard Compound

regulatory standards (Alam et al., 2021).

Table 2. Grid Box Coordinates Used for Molecular Docking Simulations

Protein	PDB ID	Box Site (x, y, z)
MAPK1	5NHV	-15.554, 13.540, 42.444
TNF-α	2AZ5	-19.162, 74.451, 33.836
BACE1	4DJU	22.180, 34.099, 56.309
CASP3	3GJQ	28.642, 34.169, 12.047

2.7 Molecular Docking

Ligand preparation: the chemical structures of ligands inlcuding compounds from *C. Sumatrana* extract and standard drugs (inhibitors for targeted proteins) were retrieved from the PubChem database (https://pubchem.ncbi.nlm.nih.gov/) in Structured Data Format (SDF) using their respective Compound Identity (CID) (Table 1). The canonical SMILES notations were also collected for structural verification and conversion. All SDF files were subsequently converted to Protein Data Bank (PDB) format. Ligand preparation involved energy minimization using the MMFF94 force field with a root mean

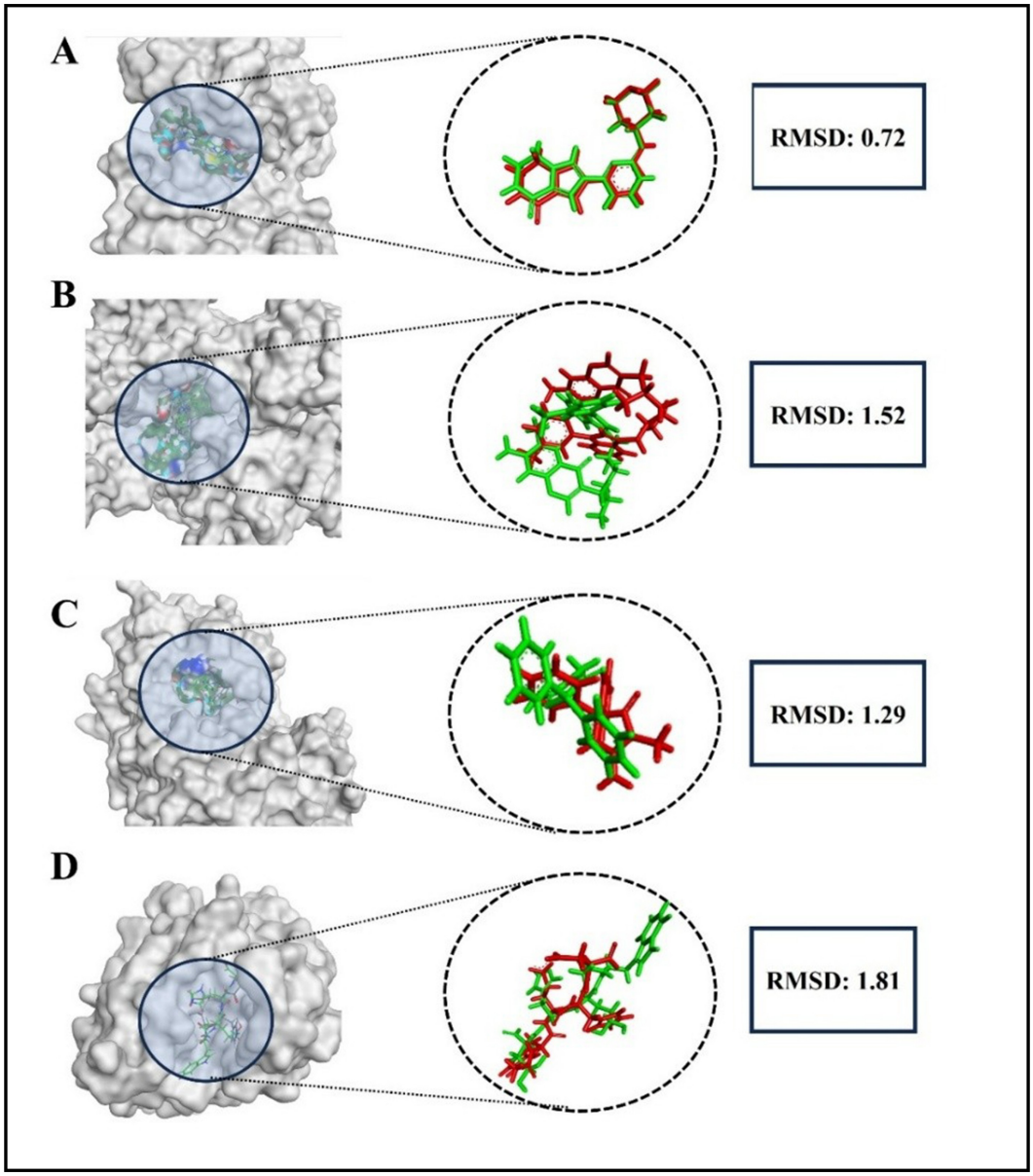

Figure 4. Visualization of Redocking of Native Ligands and Targeted Proteins. (A) MAPK1, (B) TNF-α, (C) BACE1, (D) CASP3. RMSD values <2 ÅIndicate a Valid Molecular Docking Protocol

square gradient of 0.001 kcal/mol/Å by using Open Babel (Shrestha et al., 2022).

Protein preparation: four target proteins associated with neurodegenerative diseases were selected, namely MAPK1 (PDB ID: 5NHV), TNF-α (PDB ID: 2AZ5), BACE1 (PDB ID: 4DJU), and CASP3 (PDB ID: 3GJQ) (Table 2). The corresponding crystal structures were obtained from the RCSB Protein Data Bank (https://www.rcsb.org/). Protein preparation was performed using the Molecular Operating Environment (MOE) software version 2022.02 (CCG, Montreal, Canada) by optimizing the crystal structures obtained from the PDB through removal of water molecules, addition of hydrogen atoms, and assignment of atomic charges to all protein atoms.

Molecular docking: docking simulations using MOE employed the induced fit protocol, with ligand placement performed using the Triangle Matcher/London dG method and refinement using the Force field/GBVI-WSA dG scoring function. A total of 30 docking poses were generated, and the five best-ranked poses were selected for further analysis (Senobari

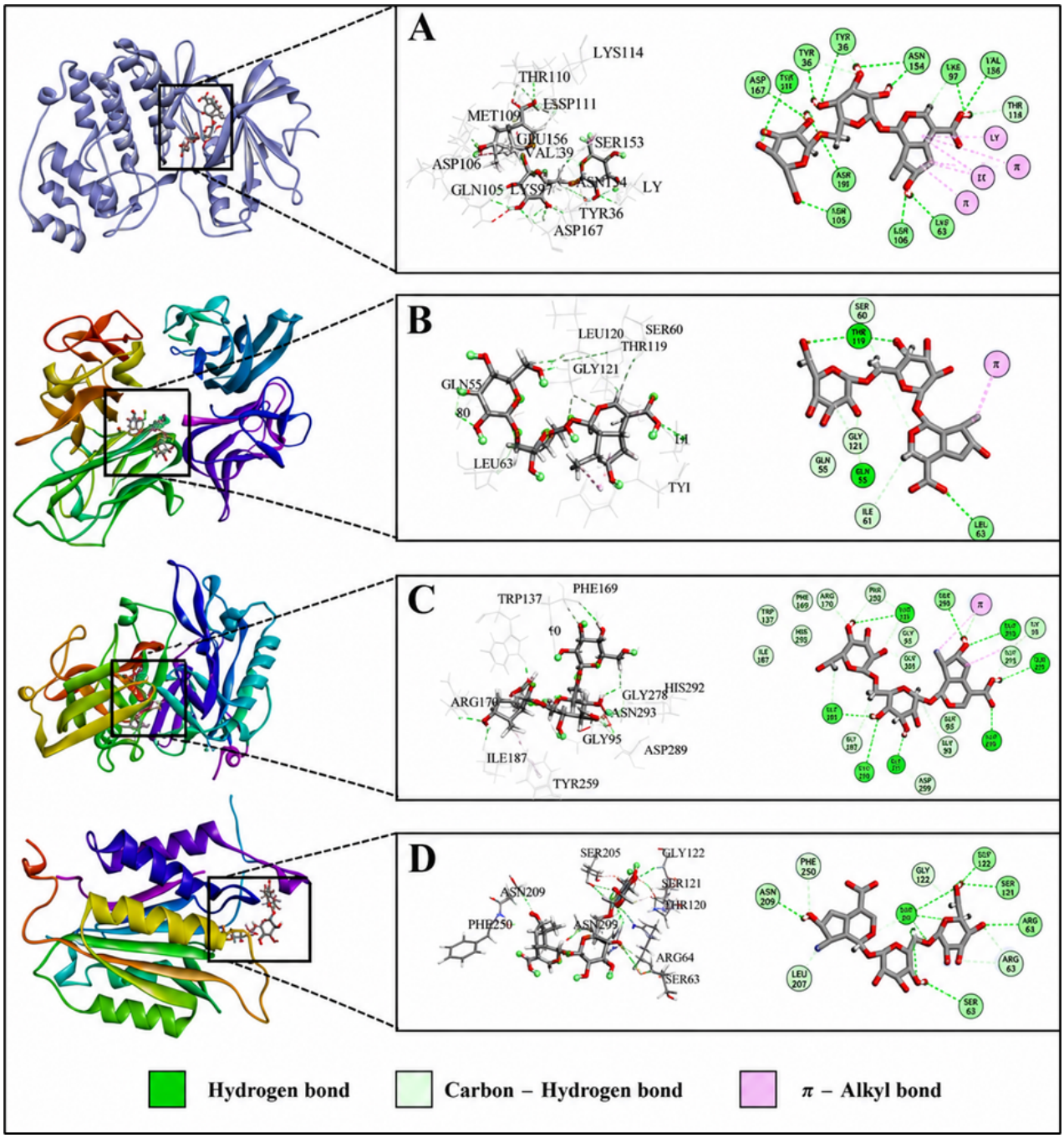

Figure 5. Molecular Docking Visualization of the Most Potent Ligands from *C. sumatrana* Extract and Targeted Proteins Involved in Neurodegenerative Diseases. (A) Interaction Between MAPK1 and Brefeldin A, (B) TNF-α and Nigakilactone K, (C) BACE1 and Genestein, (D) CASP3 and 8-Epi-Loganic acid-6'-O-beta-D-glucoside

et al., 2023). The docking complexes generated from molecular docking simulations were subjected to interaction energy analysis to estimate the contribution of steric, electrostatic, hydrogen bonding, hydrophobic, and non-covalent interactions toward ligand binding stability. The final binding energy decomposition values were expressed in kcal/mol and reported as energetic contributions of steric interactions, hydrogen bonding/electrostatic interactions, hydrophobic interactions, and non-covalent stabilization toward the total binding affinity of each ligand–protein complex. In addition, to validate the docking methodology, native ligands of each protein were subjected to redocking, with root mean square deviation (RMSD) values below 2.0 Åindicating that the docking approach used was reliable (Ramírez and Caballero, 2018).

Table 3. Selective Phytochemical Compounds of *C. sumatrana* Ethanolic Extract Determined by LC-MS/MS-QTOF

Compound Name	Group	Formula	RT (min)	Mol. Mass (Dalton)	Total Fragments	Isotope Match	Response
Fawcettimine	Alkaloids	$C_{18}H_{29}NO_3$	13.45	308.2216	7	1.77	16983
Guanine	Alkaloids	$C_5H_5N_5O$	0.6	152.0571	1	3.05	319
Genistein	Flavonoids	$C_{15}H_{12}O_5$	14.07	273.0745	2	4.32	1937
Artemisic acid	Flavonoids	$C_{15}H_{22}O_2$	7.55	235.1691	5	0.78	2615
Brefeldin A	Terpenoids	$C_{16}H_{24}O_4$	10.07	281.1747	4	0.56	1648
Furanodiene	Terpenoids	$C_{15}H_{20}O$	12.39	217.158	13	3.28	2555
Alpha-khusinol	Terpenoids	$C_{15}H_{24}O$	13.02	221.1894	25	2.55	5119
Linderazulene	Terpenoids	$C_{15}H_{14}O$	16.01	211.1107	5	4.41	1671
Loganic acid-6'-O-beta-D-glucoside	Terpenoids	$C_{22}H_{34}O_{15}$	6.72	539.1951	2	3.38	452
Pterosin Y	Terpenoids	$C_{15}H_{20}O_5$	5.01	281.1377	8	2.28	1635
Dendronobilin F	Terpenoids	$C_{15}H_{22}O_5$	5.56	281.1395	2	4.48	1464
Nigakilactone K	Terpenoids	$C_{22}H_{30}O_7$	12.27	405.1907	4	0.71	6523
Picrasin G	Terpenoids	$C_{21}H_{28}O_7$	11.18	391.175	5	0.94	6831

2.8 *In Vitro* Antioxidant Assays

The free radical scavenging potential of *C. sumatrana* extract (ECS) was evaluated using the DPPH method (Hasballah et al., 2026). ECS at concentrations of 50, 100, 250, and 500 μg/mL or ascorbic acid as a standard at concentrations of 5, 10, 20, 40, and 50 µg/mL were tested for their ability to inhibit DPPH radicals. Briefly, 2.0 mL of sample solution (ECS or ascorbic acid) was combined with 2.0 mL of 100 μg/mL DPPH solution. After vigorous agitation, the mixture was incubated in darkness at ambient temperature for 30 minutes. Furthermore, the absorbance was determined at 517 nm using a UV-Vis spectrophotometer (Thermo Fisher Scientific, USA). Antioxidant capacity (% radical scavenging activity; RSA) was calculated using a standard curve and IC50 values were extrapolated via linear regression.

ABTS radical scavenging activity of ECS was assessed using the ABTS+decolorization method (Hussen and Endalew, 2023). $ABTS^+$ radicals were synthesized by reacting 5 mL of 7 mM ABTS with 88 μL of 140 mM potassium persulfate, followed by 16-hour dark incubation. The solution was diluted with ethanol to attain an absorbance of 0.7 at 734 nm. For testing, 10 μL of sample of ECS at concentrations of 25, 50, 100, and 200 μg/mL or trolox as standard at concentrations of 6.25, 12.5, 25, 50, and 100 μg/mL was mixed with 290 μL diluted $ABTS^+$ solution in a 96-well plate and incubated in darkness for 6 minutes. Absorbance was measured at 734 nm using UV-Vis spectrophotometer. Antioxidant capacity (% radical scavenging activity; RSA) was calculated using a standard curve and IC_{50} values were extrapolated via linear regression.

The FRAP (Ferric Reducing Antioxidant Power) assay was also performed to analyze the reducing power of ECS according to Spiegel et al. (2020). In a 96-well plate, 20 μL of ECS sample at concentrations of 6.25, 12.5, 25, 50, 100 μg/mL or ascorbic acid as a standard at concentrations of 7.8125, 15.625, 31.25, 62.5, and 125 μg/mL were reacted with 280 μL FRAP reagent and incubated at 37 °C for 10 minutes. Absorbance was measured at 593 nm using a UV-Vis spectrophotometer. A standard curve was used to convert absorbance to relative reducing power (RP). RP50 values were determined via linear regression.

2.9 *In Vivo* Study on Animal Models

2.9.1 Procurement of Animal Models and Treatments

The protocols for animal use in this experiment have been approved by the Committee of Research Ethics (No.231/A/N.11-/UA/2025). Adult male mice (n = 25; BALB/c strain; 20-25 g of body weight) were provided by Balai Veteriner Baso West Sumatra. Prior to experimental treatment, mice were acclimated in the animal room with regulated temperature, humidity, and dark/light-cycle (260C, 67-68%; 12/12-h, respectively) for seven consecutive days while food (Ratbio), and drinking water (tap water) were provided ad libitum. Furtermore, mice were randomly divided equally into five groups such as control group (without any treatments), MSG-fed group (treated with 2.5 g/kg BW of monosodium glutamate only), and MSG combined with ECS at doses of 75, 150, and 300 mg/kg BW, respectively. MSG was provided in drinking water bottle continously during 28-day treatment following a previously established protocol (John et al., 2022). ECS was diluted in 1% carboxyl methyl cellulose and fed to mice through oral gavage on a daily basis for four weeks.

2.10 Behavioral Cognitive Tests

Cognitive tests were carried out according to previously described procedures (Sudhishma et al., 2021). Memory intelligence was assessed using the Hebb-Williams Maze Test. Prior to testing, each animal underwent a 3-day training period (20 min/day) within the maze apparatus. The primary parameter measured was the time required for the animal to traverse the maze from the entry to the exit. Testing was conducted during the mice's active period (4:30 PM) to align with their circadian rhythm. Spatial intelligence was evaluated via the Morris Water

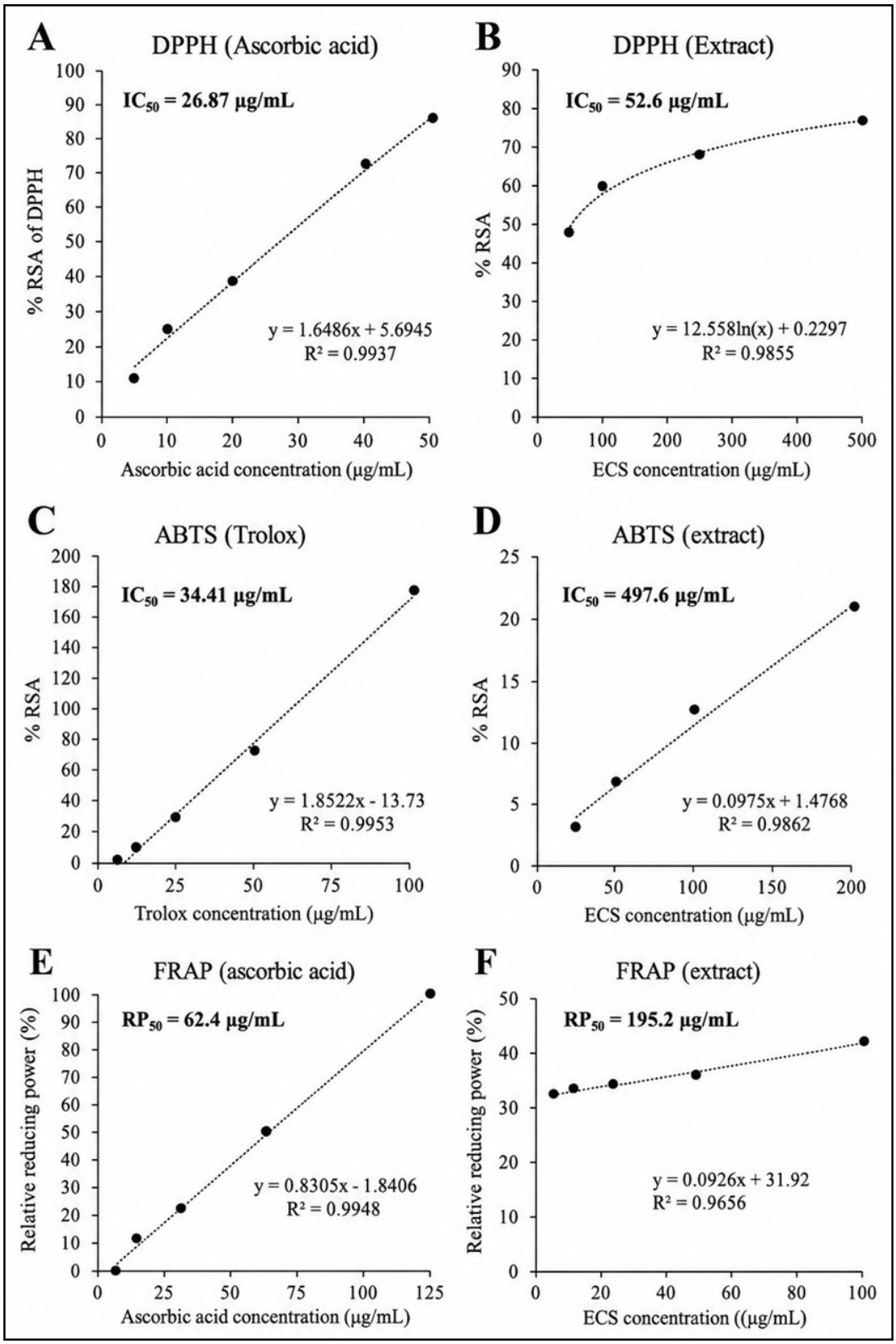

Figure 6. *In Vitro* Antioxidant Activity of Standard Compounds and *C. sumatrana* Extract (ECS) Based on DPPH Assay, ABTS Assay, and FRAP Assay. RSA (Radical Scavenging Activity), IC (Inhibitory Concentration), RP (Relative Reducing Power)

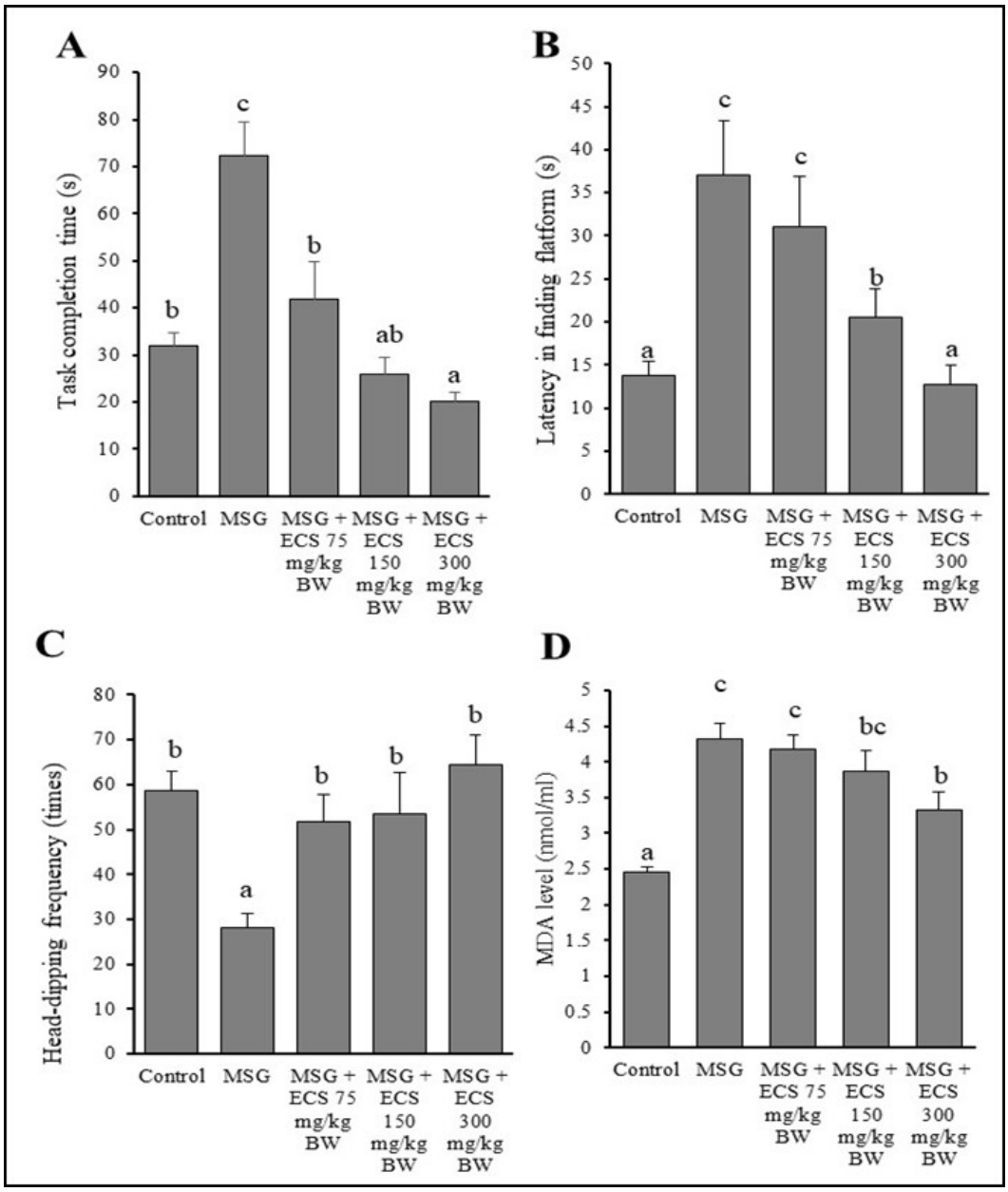

Figure 7. Effect of *C. sumatrana* Extract (ECS) on Cognitive Function and Oxidative Stress of High-MSG-Fed Mice. (A) Completion Time of Mice in Hebb-William Maze Test. (B) Latency Finding Flatform of Mice in Morris-Water Maze Test. (C) Head-Dipping Frequency of Mice in Hole Board Test. (D) MDA Levels in Brain Tissue of Mice After 28-Day Treatment. Notations (a,b,c) Letters Above the Bars Refer to Significant Differences Statistically. Data are Presented as Mean ± SD

Maze. During a 30-min pre-test training phase, the platform was positioned 1 inch above the water surface to familiarize mice with its location. For the actual test, the platform was submerged just below the water surface. Mice were released into a designated quadrant, and escape latency (time taken to reach the platform) was recorded. Exploratory behavior was analyzed using the Hole-Board Test. The number of head dips into the holes (frequency) during a 5-min observation period was quantified as the primary parameter.

2.10.1 Malondialdehyde (MDA) Measurements

The concentration of MDA in the brain tissue was analyzed according to previously described protocols (Santoso et al., 2023). Brain tissues in the area of cerebrum were harvested immediately following euthanasia of the mice. For each animal, 0.25 g of tissue was weighed, rapidly frozen, and stored at -80°C. The frozen samples were homogenized in phosphate-buffered saline with a Tissueruptor II homogenizer (Qiagen, Germany), followed by centrifugation at 5000 rpm for 15 min. MDA

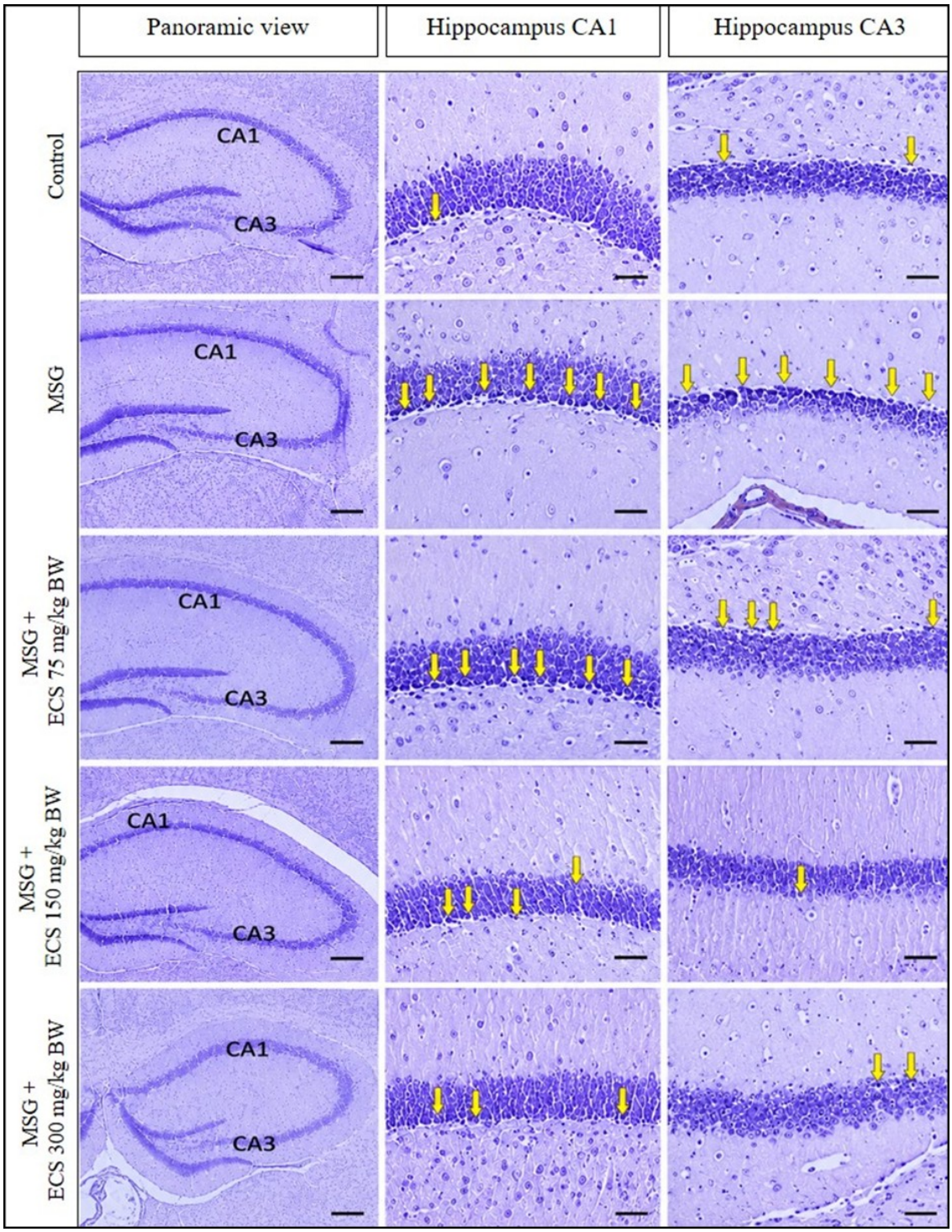

Figure 8. Effect of *C. sumatrana* Extract (ECS) on Histopathological Features of Hippocampus in the Area of Cornu Ammonis (CA1 and CA3). Left Panels are Lower Magnification (Panoramic Feature of Hippocamus; 40×). Middle and Right Panels are Higher Magnified Area (400×) of CA1 and CA3. Yellow Arrows Indicate Degenerated Cells. Scale Bars: 100 μm

levels were quantified using a commercial lipid peroxidation assay kit. Absorbance readings were obtained with a UV-Vis spectrophotometer to determine MDA concentrations.

2.10.2 Histopathological Examinations of the Brain

Brain tissues were harvested and immersed in neutral buffered formalin for 24 hours for fixation. The samples underwent dehydration through a graded alcohol series, followed by xylene

Table 4. Spectrum of Bioactivity of Compounds from *C. sumatrana* Extract Based on PASS Online Test

Compound	Activity	Probability of Activity (Pa)	Probability of Inactivity (Pi)	Criteria of Activity
Fawcettimine	Neuroprotective	0.62	0.18	Moderate
	Anti-inflammatory	0.58	0.22	Moderate
	Antioxidant	0.41	0.36	Low
	Antineurodegenerative	0.54	0.24	Moderate
	Acetylcholinesterase inhibitor	0.67	0.15	Moderate
Guanine	Antioxidant	0.36	0.48	Low
	Neuroprotective	0.33	0.51	Low
	Anti-inflammatory	0.28	0.57	Low
	Anti-Alzheimer's	0.3	0.55	Low
Genistein	Antioxidant	0.89	0.01	High
	Anti-inflammatory	0.86	0.02	High
	Neuroprotective	0.78	0.05	High
	Antineurodegenerative	0.74	0.07	High
	Anti-Alzheimer's	0.71	0.09	High
	Anti-apoptotic	0.75	0.08	High
Artemisic acid	Anti-inflammatory	0.73	0.08	High
	Antioxidant	0.52	0.28	Moderate
	Neuroprotective	0.55	0.25	Moderate
	Antineurodegenerative	0.48	0.34	Low
Brefeldin A	Anti-inflammatory	0.69	0.11	Moderate
	Anti-apoptotic	0.61	0.19	Moderate
	Neuroprotective	0.5	0.29	Moderate
	Antioxidant	0.44	0.37	Low
Furanodiene	Anti-inflammatory	0.77	0.06	High
	Neuroprotective	0.59	0.21	Moderate
	Antioxidant	0.46	0.34	Low
	Antineurodegenerative	0.53	0.27	Moderate
Alpha-khusinol	Anti-inflammatory	0.72	0.09	High
	Antioxidant	0.57	0.23	Moderate
	Neuroprotective	0.6	0.22	Moderate
	Anti-Alzheimer's	0.51	0.3	Moderate
Linderazulene	Antioxidant	0.68	0.12	Moderate
	Anti-inflammatory	0.75	0.07	High
	Neuroprotective	0.63	0.17	Moderate
	Antineurodegenerative	0.55	0.25	Moderate
8-Epi-loganic acid-6'-O-β-D-glucoside	Antioxidant	0.71	0.1	High
	Neuroprotective	0.66	0.16	Moderate
	Anti-inflammatory	0.62	0.19	Moderate
	Anti-Alzheimer's	0.58	0.23	Moderate
Pterosin Y	Antioxidant	0.64	0.17	Moderate
	Anti-inflammatory	0.61	0.2	Moderate
	Neuroprotective	0.56	0.26	Moderate

Dendronobilin F	Anti-inflammatory	0.76	0.06	High
	Neuroprotective	0.69	0.12	Moderate
	Antioxidant	0.6	0.2	Moderate
	Anti-apoptotic	0.65	0.18	Moderate
Nigakilactone K	Anti-inflammatory	0.81	0.04	High
	Neuroprotective	0.72	0.09	High
	Antineurodegenerative	0.7	0.11	Moderate
	Antioxidant	0.55	0.26	Moderate
Picrasin G	Anti-inflammatory	0.83	0.03	High
	Neuroprotective	0.74	0.08	High
	Antineurodegenerative	0.72	0.09	High
	Antioxidant	0.58	0.24	Moderate

Table 5. Assessment of Drug-Likeness Characteristics of Of Selective Phytochemical Compounds from *C. Sumatrana* Extract by Lipinski's Rule of Five Test

Compound	Characteristics based on Lipinski Rule of Five					
	Mol. Weight (≤500 Dalton)	LogP (≤5)	Hydrogen Donor (≤5)	Hydrogen Acceptor (≤10)	Molar Refractivity (40-130)	Rule Violation (≤1)
Fawcettimine	307	2.18	1	3	72.42	0
Guanine	151	-0.9	4	5	37.33	1
Genistein	270	2.41	3	5	70.81	0
Artemisic acid	234	3.64	1	2	68.63	0
Brefeldin A	280	1.96	2	4	75.91	0
Furanodiene	216	4.35	0	1	67.6	0
Alpha-khusinol	220	3.55	1	1	68.06	0
Linderazulene	232	4.3	0	0	68.4	0
8-Epi-Loganic acid-6'-O-beta-D-glucoside	538	-4.41	5	9	114.84	1
Pterosin Y	280	0.25	4	5	72.37	0
Dendronobilin F	282	-0.07	3	5	68.4	0
Nigakilactone K	406	1.37	2	7	102.46	0
Picrasin G	392	1.15	2	7	96.76	0

clearing and paraffin infiltration. The tissues were embedded in paraffin blocks, trimmed, and sectioned at 5 μm thickness with a rotary microtome (Leica, USA). Sections underwent staining with a hematoxylin and eosin kit. Histological sections were observed under a light microscope (Olympus, Japan) and representative images were captured for quantitative evaluation using digital image analysis with the ImageJ software (NIH, USA). From each section, five different microscopic fields were selected and examined, resulting in a total of 25 fields analyzed per brain. Histopathological changes were specifically assessed in the cornu ammonis (CA1 and CA3) regions of the hippocampus, focusing on degenerated and non-degenerated cells.

2.11 Data Analysis

Quantitative data were analyzed using Levene's test for homogeneity and Shapiro-Wilk test for normality followed by analysis of variance (ANOVA) and Bonferroni test. Significance level was set at $p < 0.05$. The statistical analysis was performed using SPSS 26 (IBM, USA). Data are presented as Mean ± SD.

3. RESULTS AND DISCUSSIONS

3.1 Phytochemical Profile of *C. sumatrana*

Selective LC-MS/MS-QTOF analysis of *C. sumatrana* ethanolic extract identified 13 phytochemical compounds categorized into alkaloids (2), flavonoids (2), and terpenoids (9), with the latter dominating the phytochemical profile (Figures 2 and 3; Table 3). Retention times (RT) ranged from 0.6 min (guanine) to

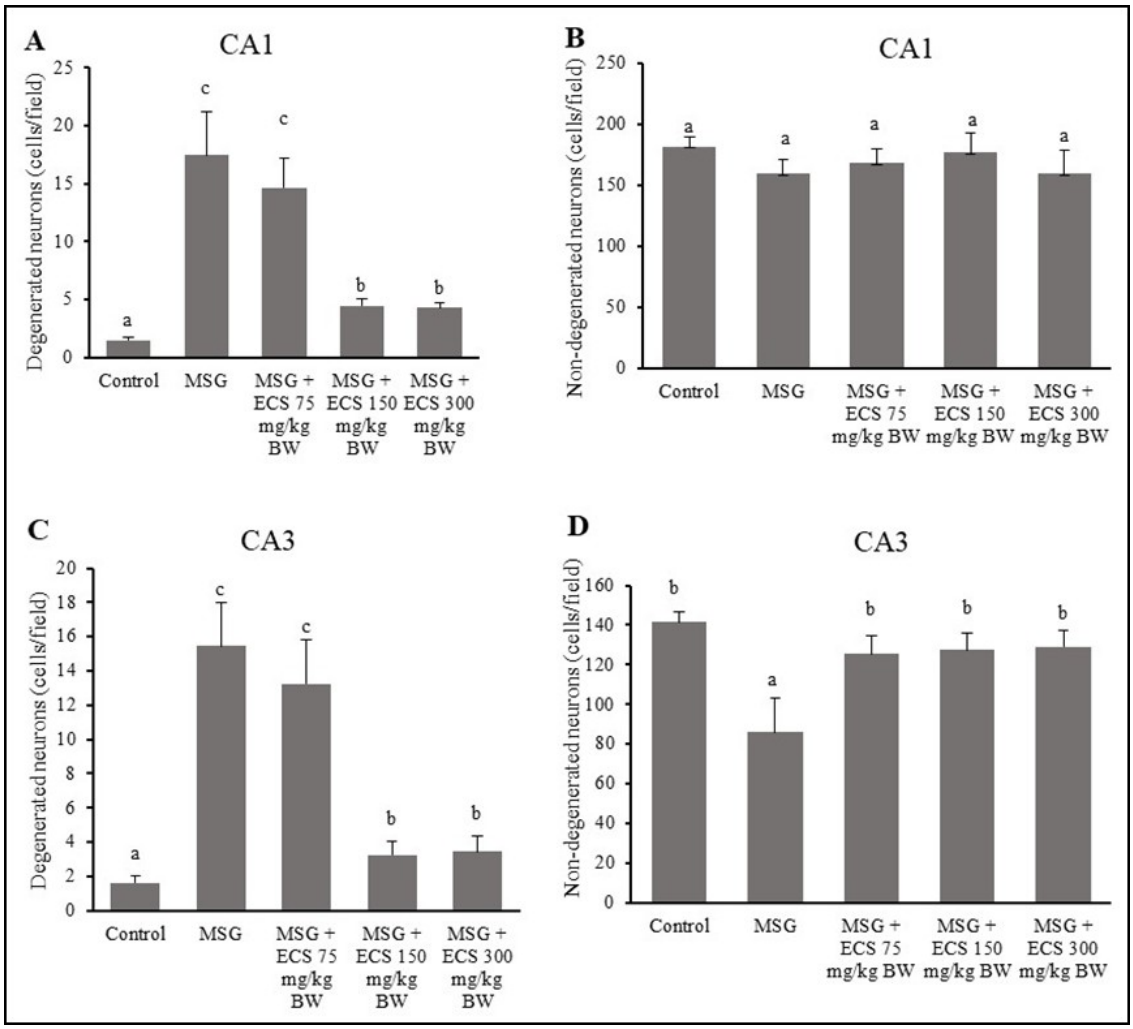

Figure 9. Effect of *C. sumatrana* Extract (ECS) on the Number of Degenerated and Non-Degenerated Neurons of Hippocampal Area of Mice. (A) Number of Degenerated Neurons in CA1 of Hippocampus. (B) Number of Non-Degenerated Neurons in CA1. (C) Number of Degenerated Neurons in CA3. and (D) Number of Non-Degenerated Neurons in CA3. Notations (a, b, c) Letters Above Each Bar Indicate Statistical Significance. Data are Presented as Mean ± SD

16.01 min (linderazulene), reflecting variability in compound polarity. Molecular masses spanned 152.0571 Da (guanine) to 539.1951 Da (loganic acid-6'-O-beta-D-glucoside), highlighting structural diversity. Total fragments per compound varied widely, from 1 (guanine) to 25 (alpha-khusinol), suggesting differences in structural complexity. Response values ranged from 319 (guanine) to 16,983 (fawcettimine), indicating significant disparities in relative abundance. The terpenoid class included compounds such as brefeldin A, furanodiene, and alpha-khusinol, with picrasin G (response 6,831) and nigakilactone K (response 6,523) exhibiting the highest responses in this group. The alkaloid fawcettimine showed the highest overall response (16,983), suggesting its prominence in the extract. However, in the present study, the compounds were only tentatively identified based on accurate mass measurements and MS/MS fragmentation patterns without quantitative validation. Therefore, this should be considered a limitation of the study, and further confirmation and quantification analyses are recommended in future investigations.

The phytochemical richness of *C. sumatrana*, particularly its terpenoid abundance (9 of 13 identified compounds), establishes a compelling foundation for its neuroprotective potential. Terpenoids like brefeldin A, alpha-khusinol, and nigakilactone K demonstrated notable structural complexity and abundance, aligning with their established roles in mitigating neurodegeneration through antioxidant, anti-inflammatory, and anti-apoptotic mechanisms in medicinal plants such as *C. kwangsiensis*, *C. longa*, and *C. zedoaria* (Elhawary et al., 2024; Zhang et al., 2024). The prominence of the alkaloid fawcettimine also highlights the importance of constituents with high bioactivity, a phenomenon observed in other neuroprotective botanicals like *Picrorhiza scrophulariiflora* (Mehla et al., 2020).

Table 6. Predictive Pharmacokinetic Properties of Compounds in *C. sumatrana* Extract

Compounds	Pharmacokinetic Properties						
	Human intestinal absorption (%)	CaCo-2 permeability (x10^{-6} cm/s)	Bioavailability score	CYP2D6 substrate	CYP2D6 inhibitor	Renal OCT2 substrate	Log S (ESOL)
Fawcettimine	94.848	1.392	0.55 (good)	No	No	No	-2.64 (soluble)
Guanine	60.702	-0.298	0.55 (good)	No	No	No	-1.70 (soluble)
Genistein	93.387	0.9	0.55 (good)	No	No	No	-4.40 (moderately soluble)
Artemisic acid	95.706	1.6	0.85 (good)	No	No	No	-3.52 (soluble)
Brefeldin A	95.36	1.01	0.55 (good)	No	No	No	-2.85 (soluble)
Furanodiene	0.8	0.73	0.55 (good)	No	No	No	-3.73 (soluble)
Alpha-khusinol	100	1.293	0.55 (good)	No	No	No	-2.98 (soluble)
Linderazulene	80	1.2	0.55 (good)	No	No	No	-5.8 (poorly soluble)
8-Epi-Loganic acid-6'-O-beta-D-glucoside	0	-0.477	0.11 (poor)	No	No	No	-0.28 (very soluble)
Pterosin Y	72.277	0.526	0.55 (good)	No	No	No	-1.45 (very soluble)
Dendronobilin F	54.769	-0.097	0.55 (good)	No	No	No	-1.43 (very soluble)
Nigakilactone K	100	0.646	0.55 (good)	No	No	No	-2.80 (soluble)
Picrasin G	93.796	0.648	0.55 (good)	No	No	No	-2.54 (soluble)

The present study employed LC-MS/MS-QTOF analysis for qualitative phytochemical screening and tentative compound identification rather than quantitative determination of analyte concentrations. Therefore, comprehensive chromatographic validation parameters such as limit of detection (LOD), limit of quantification (LOQ), linearity, precision, and repeatability, which are typically required for fully validated quantitative analytical methods, were not the primary objective of this investigation. Compound annotation was instead supported by high-resolution mass spectrometric parameters including accurate mass measurement, isotope pattern matching, and MS/MS fragmentation profile analysis. Accordingly, the LC-MS/MS data generated in this study should be interpreted as putative or tentative metabolite identification suitable for phytochemical screening purposes, rather than definitive quantitative confirmation. Additional analytical validation using authentic standards and fully validated chromatographic methods would be required for absolute quantification and definitive structural confirmation.

3.2 Predictive Bioactivity, Drug-Likeness and ADMET Profile of Bioactive Compounds from *C. sumatrana*

PASS online prediction suggested that several bioactive compounds may possess neuroprotective-related activities, as indicated by Pa values higher than Pi values (Table 4). Among them, genistein showed high probabilities for antioxidant (Pa 0.89), anti-inflammatory (0.86), neuroprotective (0.78), antineurodegenerative (0.74), anti-Alzheimer's (0.71), and anti-apoptotic (0.75) activities. Similarly, picrasin G and nigakilactone K demonstrated high anti-inflammatory (0.83 and 0.81, respectively) and neuroprotective potentials (0.74 and 0.72), with additional strong antineurodegenerative predictions. Dendronobilin F, furanodiene, and linderazulene were predominantly anti-inflammatory (Pa 0.75–0.77) with moderate neuroprotective activity. Artemisic acid also showed high anti-inflammatory activity (0.73) but moderate neuroprotective probability. Fawcettimine presented moderate multitarget potential including AChE inhibition (0.67). In contrast, guanine exhibited uniformly low probabilities (Pa < 0.36), indicating minimal predicted neuroprotective relevance. However, these findings are based solely on computational prediction and should be interpreted as preliminary indications rather than confirmed biological activities. In line with this prediction, a previous experimental study reported that compounds such as genistein exhibited neuroprotective effects in an ouabain-induced neurotoxicity model, potentially through antioxidant, anti-inflammatory, and anti-apoptotic pathways (Arafat et al., 2025).

The drug-likeness assessment of *C. sumatrana* phytochemicals via Lipinski's Rule of Five (Table 5) revealed that all of the compounds adhered to the criteria (≤1 violation), suggesting favorable oral bioavailability potential (Chen et al., 2020). Most compounds exhibited molecular weights (MW) below 500 Da, except 8-epi-loganic acid-6'-O-beta-D-glucoside (538 Da). LogP values ranged from -4.41 (8-epi-loganic acid derivative) to 4.35 (furanodiene), with all compounds within the acceptable threshold (<5). Hydrogen bond donors (≤5) and acceptors (≤10) were compliant for most. Guanine (1 violation) exceeded no individual rule but showed borderline parameters, while molar refractivity values (37.33–114.84) aligned with typical drug-like ranges (40–130) for all except guanine. Notably, genistein, artemisic acid, brefeldin A, and terpenoids like khusinol and picrasin G demonstrated strong adherence,

Table 7. Predictive Toxicity Profile of Compounds from *C. sumatrana* Extract

Compound	LD50 (mg/kg)	Toxicity criteria				
		Toxicity Class	Hepatotoxicity	Immunotoxicity	Mutagenicity	Cytotoxicity
Fawcettimine	3	I (fatal if swallowed)	No	Yes	No	No
Guanine	800	III (toxic if swallowed)				
Genistein	2500	V (harmful if swallowed)	No	No	No	No
Artemisic acid	1000	IV (harmful if swallowed)	**Yes**	**Yes**	No	No
Brefeldin A	841	IV (harmful if swallowed)	No	**Yes**	No	No
Furanodiene	116	III (toxic if swallowed)	No	No	No	No
Alpha-khusinol	1016	IV (harmful if swallowed)	No	**Yes**	No	**Yes**
Linderazulene	1000	IV (harmful if swallowed)	**Yes**	**Yes**	No	**Yes**
8-Epi-Loganic acid-6'-O-beta-D-glucoside	2000	IV (harmful if swallowed)	No	**Yes**	No	No
Pterosin Y	1600	IV (harmful if swallowed)	No	No	No	No
Dendronobilin F	26000	VI (non-toxic)	No	No	No	No
Nigakilactone K	400	IV (harmful if swallowed)	No	**Yes**	No	No
Picrasin G	79	III (toxic if swallowed)	No	**Yes**	No	No

Table 8. RMSD and Binding Affinity Values of Selected Compounds from *C. sumatrana* Extract to Targeted Proteins Involved in Neurodegenerative Diseases Based on Molecular Docking Simulations

Compounds	Targeted Proteins							
	MAPK1		TNF-α		BACE1		CASP3	
	RMSD (Å)	Affinity (kcal/mol)	RMSD (Å)	Affinity (kcal/mol)	RMSD (Å)	Affinity (kcal/mol)	RMSD (Å)	Affinity (kcal/mol)
Fawcettimine	1.07	-7.80	0.90	-7.70	1.09	-8.00	1.21	-7.20
Guanine	1.22	-6.60	1.62	-5.50	1.32	-5.70	1.36	-5.40
Genistein	1.55	-8.30	0.83	-7.50	0.98	**-9.40**	1.78	-7.60
Artemisic acid	0.72	-8.00	1.16	-6.90	1.72	-6.90	1.08	-6.70
Brefeldin A	1.50	**-9.00**	0.72	-7.30	1.01	-7.90	1.03	-8.10
Furanodiene	1.21	-7.90	1.14	-7.10	1.02	-7.20	0.70	-6.70
Alpha-khusinol	1.13	-7.70	1.50	-7.00	1.41	-7.40	0.90	-6.50
Linderazulene	0.63	-7.20	0.57	-6.80	1.52	-5.50	1.70	-6.00
8-Epi-Loganic acid-6'-O-beta-D-glucoside	1.93	-8.20	1.39	-7.60	1.62	-8.10	1.92	**-9.00**
Pterosin Y	0.93	-7.20	1.15	-6.80	1.33	-6.70	1.42	-6.50
Dendronobilin F	1.91	-5.90	0.70	-6.60	1.66	-6.60	1.12	-6.20
Nigakilactone K	0.55	-6.90	0.65	**-8.60**	0.66	-8.50	1.85	-7.90
Picrasin G	1.24	-6.90	1.36	-8.30	1.09	-8.10	1.80	-7.80
Native inhibitor	0.72	-7.66	1.52	-7.94	1.29	-5.40	1.81	-8.12
Standard drug	1.34	-9.30	1.70	-9.00	1.63	-9.00	1.96	-8.10

highlighting their potential as orally bioavailable candidates. These results demonstrate the drug-like properties of most *C. sumatrana* compounds.

The ADME prediction results (Table 6) demonstrated that several bioactive compounds identified in the *C. sumatrana* extract possess favorable pharmacokinetic characteristics, indicating their potential suitability as drug candidates. Most compounds showed high human intestinal absorption values, including artemisic acid (95.706%), brefeldin A (95.36%), genistein (93.387%), picrasin G (93.796%), and alpha-khusinol (100%), suggesting good oral absorption potential. In agreement with these findings, the majority of compounds also exhibited positive CaCo-2 permeability values, indicating acceptable intestinal membrane permeability. Artemisic acid showed the highest bioavailability score (0.85), while most other compounds presented good bioavailability scores of 0.55, supporting their potential systemic availability following oral administration. In contrast, 8-epi-loganic acid-6'-O-beta-D-glucoside

Table 9. Binding Energy Decomposition of Selected Compounds from *C. sumatrana* Extract to Targeted Proteins Involved in Neurodegenerative Diseases Based on Molecular Docking Simulations

Protein	Compounds	Hydrogen Bond Energy (kcal/mol)	Carbon Hydrogen Energy (kcal/mol)	van der Waals/ Hydrophobic Energy (kcal/mol)	Non-Covalent Interaction Energy (kcal/mol)	Total Affinity (kcal/mol)
MAPK1	Native inhibitor	-5	-1	-1.7	–	-7.66
	Standard drug	-6	-0.8	-2.5	–	-9.3
	Artemisic acid	-3.5	-2	-2.5	–	-8
	Brefeldin A	-5.5	-0.6	-2.9	–	-9
	Dendronobilin F	-3.5	-0.5	-1.9	–	-5.9
	Fawcettimine	-3.5	-0.8	-3.5	–	-7.8
	Furanodiene	0	0	-7.9	–	-7.9
	Genistein	-6.2	-0.5	-1.6	–	-8.3
	Guanine	-5	0	-1.6	–	-6.6
	Alpha-khusinol	-2	0	-5.7	–	-7.7
	Linderazulene	0	0	-7.2	–	-7.2
	8-Epi-Loganic acid-6'-O-beta-D-glucoside	-6.8	-0.4	-1	–	-8.2
	Nigakilactone K	-3.5	-1	-2.4	–	-6.9
	Picrasin G	-3	-0.7	-3.2	–	-6.9
	Pterosin Y	-5.5	0	-1.7	–	-7.2
TNF-α	Native inhibitor	-2.5	-0.8	-3	-1.6	-7.94
	Standard drug	-2.5	-0.5	-6	–	-9
	Artemisic acid	-4	-0.5	-2.4	–	-6.9
	Brefeldin A	-2	0	-5.3	–	-7.3
	Dendronobilin F	-2.5	0	-4.1	–	-6.6
	Fawcettimine	-2	-0.7	-5	–	-7.7
	Furanodiene	0	0	-7.1	–	-7.1
	Genistein	-4	0	-3.5	–	-7.5
	Guanine	-4	0	-1.5	–	-5.5
	Alpha-khusinol	0	0	-7	–	-7
	Linderazulene	0	-0.5	-6.3	–	-6.8
	8-Epi-Loganic acid-6'-O-beta-D-glucoside	-4.5	-1.2	-1.9	–	-7.6
	Nigakilactone K	-2	-1	-5.6	–	-8.6
	Picrasin G	-2.5	0	-5.8	–	-8.3
	Pterosin Y	-4.5	-0.5	-1.8	–	-6.8
BACE1	Native inhibitor	0	-0.5	-4.9	–	-5.4
	Standard drug	-5.5	-0.7	-2.8	–	-9
	Artemisic acid	0	0	-6.9	–	-6.9
	Brefeldin A	-4	-0.5	-3.4	–	-7.9
	Dendronobilin F	-2.5	-0.5	-3.6	–	-6.6
	Fawcettimine	-2	0	-6	–	-8
	Furanodiene	0	0	-7.2	–	-7.2
	Genistein	-5.5	-0.5	-3.4	–	-9.4
	Guanine	-5	0	-0.7	–	-5.7
	Alpha-khusinol	0	0	-7.4	–	-7.4
	Linderazulene	0	0	-5.5	–	-5.5
	8-Epi-Loganic acid-6'-O-beta-D-glucoside	-6	-0.6	-1.5	–	-8.1
	Nigakilactone K	-3.5	-1.2	-3.8	–	-8.5
	Picrasin G	0	-0.8	-7.3	–	-8.1
	Pterosin Y	-5.5	-0.5	-0.7	–	-6.7

CASP3	Native inhibitor	-5	-0.7	-1	-1.4	-8.12
	Standard drug	-6	-0.5	-1.6	–	-8.1
	Artemisic acid	-3.5	0	-3.2	–	-6.7
	Brefeldin A	-4	-0.6	-3.5	–	-8.1
	Dendronobilin F	-2.5	-0.5	-3.7	–	-6.2
	Fawcettimine	-2	0	-5.2	–	-7.2
	Furanodiene	0	-0.5	-4.5	-1.7	-6.7
	Genistein	-4.2	0	-2	-1.4	-7.6
	Guanine	-3.8	0	-0.6	-1	-5.4
	Alpha-khusinol	0	-0.5	-6	–	-6.5
	Linderazulene	0	0	-4.4	-1.6	-6
	8-Epi-Loganic acid-6'-O-beta-D-glucoside	-6.5	-0.8	-1.7	–	-9
	Nigakilactone K	-3.5	-0.6	-3.8	–	-7.9
	Picrasin G	-3	-0.8	-4	–	-7.8
	Pterosin Y	-4	0	-2.5	–	-6.5

demonstrated poor pharmacokinetic properties, including 0% predicted intestinal absorption, negative CaCo-2 permeability, and a low bioavailability score (0.11), suggesting limited oral bioavailability. Importantly, none of the identified compounds were predicted to act as CYP2D6 substrates or inhibitors, indicating a lower possibility of CYP2D6-mediated metabolic interactions and reduced risk of adverse drug–drug interactions. In addition, all compounds were predicted to be non-substrates of renal OCT2 transporters, suggesting minimal involvement in OCT2-mediated renal transport pathways. Solubility prediction based on Log S (ESOL) further showed that most compounds were categorized as soluble to very soluble, although genistein and particularly linderazulene displayed lower solubility profiles, with linderazulene categorized as poorly soluble. Overall, these findings suggest that several compounds from *C. sumatrana* possess promising pharmacokinetic properties that may support their biological activities and potential therapeutic application, although compounds with lower solubility or absorption may require formulation optimization to improve their bioavailability (Divyashri et al., 2021).

Predictive toxicity assessment of *C. sumatrana* compounds (Table 7) revealed variable toxicity profiles, with fawcettimine exhibiting the highest acute toxicity (LD_{50}: 3 mg/kg; Class I, fatal if swallowed) and notable immunotoxicity. Most compounds fell into Class IV (harmful if swallowed; e.g., artemisic acid, LD_{50}: 1000 mg/kg) or Class III (toxic if swallowed; e.g., furanodiene, LD_{50}: 116 mg/kg), while dendronobilin F emerged as non-toxic (LD_{50}: 26,000 mg/kg; Class VI). Hepatotoxicity was observed in artemisic acid, linderazulene, and khusinol, whereas immunotoxicity was widespread, affecting fawcettimine, artemisic acid, brefeldin A, khusinol, linderazulene, and others. Cytotoxicity was limited to khusinol and linderazulene, while mutagenicity was absent across all compounds. Notably, picrasin G (LD_{50}: 79 mg/kg; Class III) and nigakilactone K (LD_{50}: 400 mg/kg; Class IV) demonstrated moderate toxicity with immunotoxic effects. These results highlight dendronobilin F as a promising low-risk candidate, while emphasizing the need for caution with highly toxic compounds like fawcettimine and cytotoxic terpenoids. The absence of mutagenicity suggests potential for therapeutic exploration with appropriate safety mitigation.

3.3 Molecular Docking of Bioactive Compounds from *C. sumatrana* and Proteins Involved in Neurodegenerative Diseases

Molecular docking simulations were performed to reveal the plausible inhibitory interactions between bioactive compounds from *C. sumatrana* extract and proteins involved in the development and progression of neurodegenerative diseases (MAPK1, TNF-α, BACE1, and CASP3) (Table 8; Figures 4 and 5). It was validated using the docking performance of the standard drugs toward the targeted proteins. The standard drugs exhibited strong binding affinities with docking scores of -9.30, -9.00, -9.00, and -8.10 kcal/mol against MAPK1, TNF-α, BACE1, and CASP3, respectively, indicating stable ligand–protein interactions and serving as a benchmark for evaluating the tested compounds. In addition, the RMSD values of the standard drugs ranged from 1.34 to 1.96 Å, which fall within the acceptable threshold (< 2.0 Å) for reliable docking conformations, suggesting that the predicted binding poses are structurally consistent and valid. Similarly, the native inhibitors demonstrated comparable binding orientations with RMSD values between 0.72 and 1.81 Å and moderate docking scores. These results confirm that the docking protocol applied in this study is reliable and capable of reproducing stable ligand–protein interactions, thereby validating the simulation used to assess the binding potential of the investigated compounds. In addition, the molecular docking protocol was also validated by redocking the native ligand into each target protein. As shown in Figure 4, the redocking results were considered valid, as indicated by RMSD values of all native ligand–protein complexes below 2 Å.

Molecular docking analysis revealed that several compounds in *C. sumatrana* extract exhibited competitive binding affinities against neurodegenerative disease-associated proteins compared to standard drugs (inhibitors) (Tables 8 and 9; Figure 5).

Among the tested compounds, genistein showed the strongest affinity toward BACE1 with a total binding energy of -9.4 kcal/mol, exceeding the standard drug (-9.0 kcal/mol). This strong interaction was primarily supported by substantial hydrogen bond energy (-5.5 kcal/mol), together with carbon hydrogen interactions (-0.5 kcal/mol) and hydrophobic interactions (-3.4 kcal/mol), indicating stable ligand-protein binding. Genistein also demonstrated strong affinity toward MAPK1 (-8.3 kcal/mol), mainly contributed by hydrogen bonding energy of -6.2 kcal/mol, suggesting the importance of polar interactions in stabilizing the complex. Brefeldin A exhibited notable inhibitory potential against MAPK1 with a binding affinity of -9.0 kcal/mol, closely matching the standard drug (-9.3 kcal/mol). Its interaction was supported by strong hydrogen bonding energy (-5.5 kcal/mol) and hydrophobic interactions (-2.9 kcal/mol). Similarly, brefeldin A displayed equivalent binding affinity to the standard drug against CASP3 (-8.1 kcal/mol), with interaction stability contributed by hydrogen bonds (-4.0 kcal/mol), carbon hydrogen interactions (-0.6 kcal/mol), and hydrophobic energy (-3.5 kcal/mol). 8-epi-loganic acid-6'-O-beta-D-glucoside demonstrated particularly strong interaction with CASP3, exhibiting a total affinity of -9.0 kcal/mol, comparable to the standard inhibitor (-8.1 kcal/mol). This interaction was mainly dominated by high hydrogen bond energy (-6.5 kcal/mol), supported by additional carbon hydrogen interactions (-0.8 kcal/mol) and hydrophobic interactions (-1.7 kcal/mol). The same compound also showed strong binding toward MAPK1 (-8.2 kcal/mol) and BACE1 (-8.1 kcal/mol), suggesting potential multi-target inhibitory activity mediated predominantly through hydrogen bonding interactions. Nigakilactone K exhibited strong affinity toward TNF-α (-8.6 kcal/mol) and BACE1 (-8.5 kcal/mol), closely approaching the binding energies of the standard compounds. Its interaction with TNF-α was largely stabilized by hydrophobic interactions (-5.6 kcal/mol), along with hydrogen bonding (-2.0 kcal/mol) and carbon hydrogen interactions (-1.0 kcal/mol). Similarly, its binding to BACE1 involved balanced contributions from hydrogen bonding (-3.5 kcal/mol), carbon hydrogen interactions (-1.2 kcal/mol), and hydrophobic interactions (-3.8 kcal/mol). Picrasin G also displayed robust binding toward TNF-α (-8.3 kcal/mol) and BACE1 (-8.1 kcal/mol), with hydrophobic interactions representing the major stabilizing force, particularly against BACE1 (-7.3 kcal/mol). Overall, the binding energy decomposition analysis suggested that both hydrogen bonding and hydrophobic interactions played essential roles in stabilizing ligand–protein complexes.

The results of interaction recidue analysis (Table 10) indicated that within MAPK1, ligand binding was mainly characterized by hydrogen bonding with Lys54 and Asp167, key residues associated with ATP-binding and catalytic activity (Wu et al., 2025), alongside hydrophobic interactions involving Tyr36, Val39, Ile31, Ala52, and Leu156. Genistein, pterosin Y, nigakilactone K, and loganic acid derivatives showed interaction patterns comparable to the native inhibitor and commercial drug, suggesting possible occupancy of the MAPK1 active site. Moreover, in TNF-α, binding was dominated by hydrophobic and aromatic interactions with Tyr119, Tyr59, and Leu57, while hydrogen bonds with Tyr151 and Gly121 may contribute to ligand orientation. Compounds such as artemisic acid, genistein, and pterosin Y exhibited interaction profiles similar to the commercial drug, potentially indicating interference with TNF-α receptor interactions. Next, within BACE1, ligand binding relied predominantly on hydrophobic enclosure involving Trp137, Tyr259, Phe169, and Asp93, while selective hydrogen bonding with Asp93 and Ile187 was observed for compounds including genistein, guanine, and nigakilactone K, suggesting possible relevance to amyloidogenic pathways (Bartolić and Bosak, 2025). In CASP3, recurrent hydrogen bonding with Arg207, Arg64, His121, and Thr62, together with hydrophobic stabilization by Trp206, Tyr204, and Phe256, was observed across several ligands. Notably, genistein, pterosin Y, and nigakilactone K demonstrated interaction patterns comparable to the commercial drug, suggesting potential modulation of apoptotic signaling (Shi et al., 2026). However, all observations are based on molecular docking predictions and require further biochemical and experimental validation.

Molecular docking provided mechanistic insights, revealing competitive binding of key compounds in *C. sumatrana* to neurodegenerative targets. Brefeldin A showed a strong affinity to MAPK1, a signaling protein that has been shown to contribute to neurodegenerative pathology by promoting tau hyperphosphorylation, neuroinflammation, oxidative stress, and synaptic dysfunction (Wang et al., 2021). Moreover, genistein exhibited a highest affinity to BACE1, suggesting its potential to inhibit amyloid-β production, a hallmark of Alzheimer's pathology (Satir et al., 2020). Similarly, brefeldin A and nigakilactone K showed strong inhibitory interactions with CASP3 and TNF-α, implicating them in apoptosis regulation and neuroinflammation modulation-pathways central to neurodegenerative diseases (Zhang et al., 2025). These findings align with a previous *in silico* study demonstrating that curcumin from *C. longa* had a strong inhibitory interaction with TNF-α (Singh et al., 2025) while bisdemethoxycurcumin and demethoxycurcumin from *C. longa* also had an inhibitory interaction with BACE1 (Shakira and Maulina, 2025). Another molecular docking simulation indicated that nano-curcumin had an inhibitory interaction with CASP3 (Kh et al., 2025) while apigenin, demethoxycurcumin, quercetin and curcumin from *C. longa* also had a high affinity to MAPK1 to elicit inhibitory effect (Han et al., 2023).

The molecular docking findings of the present study are relevant to several FDA-approved drugs that have demonstrated clinical efficacy against neurodegenerative diseases, namely donepezil, memantine, and aducanumab. A previous study has reported that donepezil can interact with BACE1 in addition to its established acetylcholinesterase inhibitory activity (Gabr and Abdel-Raziq, 2018). Another study showed that aducanumab possesses a strong binding affinity for amyloid-β *in vitro* (Söderberg et al., 2023). In addition, memantine has been shown to modulate signaling pathways involved in excitotoxicity and

Table 10. Binding Types and Interacting Residues of Ligand–Protein Complexes Based on Molecular Docking Simulations

	MAPK		TNF-α		BACE1		CASP3	
Compounds	Binding	Residue	Binding	Residue	Binding	Residue	Binding	Residue
Native Inhibitor	Hydrogen	Asp167, Lys54, Met108	Hydrogen	Tyr C:151	Hydrogen	-	Hydrogen	Ser B:209, Arg B:207, His A:121, Gly A:122, Thr A:62
	Carbon Hydrogen	Asn154, Ser153, Asp111, Asp106	Carbon Hydrogen	Ser C:60, Gln C:61	Carbon Hydrogen	Ser96	Carbon Hydrogen	Asn B:208, Phe B:250
	Hydrophobic	Tyr36, Val39, Ile31, Ala52, Leu156, Gln105, Ile84, Leu107, Gln109, Thr110	Hydrophobic	Tyr C:59, Leu C:57, Leu D:57, Tyr D:59, Leu B:55	Hydrophobic	Ile179, Gly291, Asp93, Ile287, Asp289, Thr292, Gly95, Tyr259, Ile287, Arg189, Val130, Pro131, Trp137, Phe169, Tyr132	Hydrophobic	Ser B:249, Trp B:214, Glu B:248, Ser A:65, Ser A:63, Gly A:60, Phe A:128, Glu A:123, Met A:61, Ser B:205, Tyr B:204, Arg A:64, Gln A:161, Phe B:256, Leu A:168, Trp B:206
			Non-Covalent Interaction	Tyr D:119, Tyr C:119			Non-covalent interaction	Lys A:163
Commercial Drug	Hydrogen	Lys54, Gln105, Asp167, Asp111	Hydrogen	Gly C:122	Hydrogen	Tyr259, Ile187, Asp93	Hydrogen	Arg B:207, Thr A:62, His A:121, Cys A:163, Ser A:65
	Carbon Hydrogen	Lys151, Gln105,	Carbon Hydrogen Bond	Leu D:120	Pi-Donor Hydrogen Bond	Trp137	Carbon Hydrogen	Phe B:250, Ser 205
	Hydrophobic	Cys166, Leu156, Ala52, Val39, Ile31	Hydrophobic	C:120, Tyr D:119, Tyr C:119, Gly D:121, Leu B:55, Ile D:58, Gly D:122, Leu B:157, Leu D:57, Tyr C:59, Ile D:155, Val C:123, Leu C:57, Tyr D:59, Gly C:121, Tyr D:151, Gln D:61, Ser D:60, Leu	Hydrophobic	Arg189, Pro131, Val130, Ser97, Asn98, Ser96, Phe169, Trp176, Ile171, Leu91, Ile179, Gly291, Tyr132, Gly95	Hydrophobic	Asn B:206, Trp B:206, Tyr B:204, Gly A:60, Met A:61, Gln A:161, Arg A:64, Ser A:120, Ala A:162, Gly A:122, Tyr B:204, Phe B:256, Ser B:251, Ser B:209, Ser B:249, Trp B:214
Artemisic acid	Hydrogen	Gln105, Lys54	Hydrogen	Ser D:60, Tyr D:151, Gly C:121	Hydrogen	-	Hydrogen	Cys A:163, Arg B:207, Arg A:64
	Carbon Hydrogen	Leu107, Asp106, Val104, Ile53, Ile103, Gly71, Asp167, Tyr36, Asp11, Asn154, Ser153, Ile31	Carbon Hydrogen	Leu C:120	Carbon Hydrogen	-	Carbon Hydrogen	-
	Hydrophobic	Met108, Ala52, Ile84, Leu156, Val39, Cys166	Hydrophobic	Leu D:57, Tyr C:59, Tyr C:151, Ser C:60, Tyr C:119, Gln D:61, Tyr D:119, Leu D:120, Gly D:121, Tyr D:59, Leu C:57, Gly C:122, Ile D:155	Hydrophobic	Arg189, Val130, Trp137, Phe169, Leu91, Tyr132, Ile179, Tyr259, Gly291, Asp289, Thr292, Gly95, Asp93, Ser96	Hydrophobic	Ser B:205, Phe B:256, Trp B:206, Tyr B:204, Thr A:62, His A:121, Ser A:120, Ala A:161, Gln A:161
Brefeldin A	Hydrogen	Asp167, Lys54	Hydrogen	Tyr D:151	Hydrogen	Tyr259, Ile187	Hydrogen	Arg A:64, Arg B:207
	Carbon Hydrogen	Ser153	Carbon Hydrogen	-	Carbon Hydrogen	Ser96	Carbon Hydrogen	Ser A:120
	Hydrophobic	Lys151, Asp111, Ile31, Leu107, Asp106, Gln105, Tyr35, Cys166, Val39, Leu156, Ala52, Met108, Ile84	Hydrophobic	Tyr D:59, Gly C:121, Gly C:122, Leu C:120, Tyr C:119, Ser C:60, Tyr C:59, Gln C:61, Tyr C:151, Gly D:121, Leu D:120, Tyr D:119, Gln D:61, Ser D:60	Hydrophobic	Ile179, Trp137	Hydrophobic	Ser B:205, Ala A:162, Gly A:122, Thr A:62, Trp B:206, Tyr B:204, Phe B:256, Leu A:168
Dendronobilin F	Hydrogen	Tyr 36, Ser153	Hydrogen	Gly C:121	Hydrogen	Trp137	Hydrogen	Arg B:207
	Carbon Hydrogen	Tyr36	Carbon Hydrogen	-	Carbon Hydrogen	Gly291	Carbon Hydrogen	His A:121
	Hydrophobic	Lys54, Asp167, Asn154, Met108, Ile31, Asp111, Lys114, Thr110, Val39, Glu33, Gly32, Leu156, Cys166	Hydrophobic	Gly D:121, Leu D:120, Ile D:155, Leu D:57, Ser D:60, Tyr D:59, Leu C:57, Gly C:122, Tyr C:59, Tyr D:151, Gln D:61, Leu C:120, Tyr D:119, Tyr C:119	Hydrophobic	Trp176, Ile171, Phe169, Leu91, Ile179, Asp93, Val130, Gly95, Ser96	Hydrophobic	Tyr B:204, Phe B:256, Trp B:206, Arg A:64, Gln A:161, Thr A:62, Ser B:205
Fawcettimine	Hydrogen	Lys54, Ser153	Hydrogen	Gly C:122	Hydrogen	Gly291	Hydrogen	Arg B:207
	Carbon Hydrogen Bond	Asp167	Carbon Hydrogen Bond	Leu D:120	Carbon Hydrogen Bond	-	Carbon Hydrogen Bond	-
	Hydrophobic	Ala52, Leu156, Tyr36, Val39, Cys166	Hydrophobic	Leu D:57, Tyr C:59, Ile D:155, Val C:123, Leu C:57, Tyr D:59, Gly C:121, Tyr D:151, Gln D:61, Ser D:60, Leu C:120, Tyr D:119, Tyr C:119, Gly D:121, Leu B:55, Ile D:58, Gly D:122, Leu B:157	Hydrophobic	Asp93, Thr133, Gly95, Tyr259, Ser96, Trp137, Val130, Phe169, Trp176, Lys168, Tyr132, Asp289, Ile179, Thr292, Leu91	Hydrophobic	Ser A:65, Tyr B:204, Phe B:256, Cys A:163, Trp B:206, Ser B:205, Gln A:161, Ser A:120, Ala A:162, Arg A:64, Gly A:122, His A:121, Thr A:62
Furanodiene	Hydrogen	-	Hydrogen	-	Hydrogen Bond	-	Hydrophobic	Arg A:64, Thr A:62, Arg B:207, Ser B:205, Phe B:256, Tyr B:204, Leu A:168, His A:121
	Carbon Hydrogen	-	Carbon Hydrogen	-	Carbon Hydrogen	-	Carbon Hydrogen	Trp B:206
	Hydrophobic	Ile31, Leu156, Ala52, Ile84, Cys166, Tyr36, Lys54, Val39	Hydrophobic	Tyr C:119, Tyr D:119, Ser C:60, Gln C:61, Tyr C:151, C:59, Leu C:120, Gln D:61, Gly C:121, Tyr D:151, Ser D:60, Gly C:122, Tyr D:59, Leu D:120, Gly D:121	Hydrophobic	Tyr132, Phe169, Val130, Asn98, Trp137, Ile179, Ser96, Arg189, Ile187, Gly95, Tyr259, Asp93	Non-covalent interaction	Cys A:163
Genistein	Hydrogen	Met108, Asp111, Lys114	Hydrogen	Gly C:121, Tyr D:151	Hydrogen	Ile187, Gly291	Hydrogen	Arg A:64, Ser A:120, Phe B:256
	Carbon Hydrogen	Thr110	Carbon Hydrogen	-	Carbon Hydrogen	Ser96	Hydrophobic	Tyr B:204, His A:121, Gly A:122, Ala A:162, Gln A:161, Ser B:213, Ser B:205, Trp B:206
	Hydrophobic	Glu71, Asp167, Lys54, Cys166, Val39, Leu156, Glu109, Leu107, Ala52, Gln105, Ile103	Hydrophobic	Leu B:157, Val B:123, Val D:123, Leu B:55, Gly D:122, Leu D:57, Gly D:121, Leu D:120, Tyr D:122, Leu D:57, Tyr D:119, Ser D:60, Gln D:61, Leu C:120, Gly C:122	Hydrophobic	Ala188, Arg189, Ser97, Asn98, Val130, Trp137, Tyr132, Phe169, Trp176, Ile171, Leu91, Ile179, Thr292, Asp93	Non-covalent interaction	Cys A:163, Arg B:207

Guanine	Hydrogen	Gln105, Asp106, Met108	Hydrogen	Tyr D:151, Gly C:121	Hydrogen Bond	Ile187, Asn98, Trp137	Hydrogen	Ser A:120, Arg A:64, His A:121
	Carbon Hydrogen	-	Carbon Hydrogen	-	Carbon Hydrogen	-	Hydrophobic	Trp B:206, Ser B:205, Gln A:161, Ala A:162, Gly A:122
	Hydrophobic	Ile84, Val39, Ala52, Cys166, Leu156, Ile31, Leu107	Hydrophobic	Leu D:57, Tyr D:59, Gly C:122, Leu C:120, Gln D:61, Tyr D:119, Ser D:60, Leu D:120, Gly D:121, Gly D:122	Hydrophobic	Ala188, Arg189, Val130, Tyr132, Phe169, Ile179, Ser96, Ser97	Non-covalent interaction	Arg B:207, Cys A:163
Alpha-Khusinol	Hydrogen	Lys54	Hydrogen	-	Hydrogen	-	Hydrogen	-
	Carbon Hydrogen	-	Carbon Hydrogen	-	Carbon Hydrogen	-	Carbon Hydrogen	His A:121
	Hydrophobic	Ile53, Ala52, Ile31, Val39, Leu107, Met108, Asp111, Leu156, Ser153, Tyr36, Asp167, Asn154	Hydrophobic	Tyr C:119, Gly D:121, Leu B:55, Leu B:157, Gly D:122, Val B:123, Val D:123, Leu D:57, Tyr D:59, Gly C:122, Gly C:121, Leu C:57, Tyr D:151, Ser D:60, Leu D:120, Tyr D:119	Hydrophobic	Phe169, Asp93, Trp137, Ile179, Asn98, Val130, Ser96, Arg189, Ile187, Gly291, Gly95, Tyr132, Thr133	Hydrophobic	Tyr B:204, Gly A:122, Cys A:163, Trp B:206, Thr A:62, Ser B:205, Arg B:207, Ser B:213, Gln A:161, Ala A:162, Arg A:64, Ser A:120
Linderazulene	Hydrophobic	Leu156, Cys166, Val39, Tyr36, Ile84, Ala52, Lys54	Hydrogen	-	Hydrogen	-	Hydrogen	-
	Carbon Hydrogen	-	Carbon Hydrogen	Gly C:121	Carbon Hydrogen	-	Hydrophobic	Trp B:206, Ser B:205, Ser B:213, Gln A:161, Arg A:64, Ser A:120, His A:121, Ala A:162, Gly A:122, Tyr B:204
	Hydrophobic	Ser153, Tyr36, Val39, Leu156, Ile31, Ile84, Met108, Leu107, Asp106, Gln105, Glu71, Lys54, Asp167, Cys166	Hydrophobic	Tyr D:119, Gln D:61, Ser D:60, Leu D:120, Gly C:122, Tyr D:59, Ile D:155, Tyr D:151, Leu D:57, Val C:123, Leu C:57, Tyr C:59, Ser C:60, Tyr C:119, Leu C:120, Tyr C:151	Hydrophobic	Asp289, Ser96, Gly95, Thr292, Gly291, Asp93, Ile179, Leu91, Trp176, Ile171, Phe169, Tyr132, Trp137, Val130	Non-covalent interaction	Arg B:207, Cys A:163
Loganic acid 6'-O-beta-D-glucosid	Hydrogen	Lys151, Ser153, Asp167, Lys54, Gln105, Asp111, Lys114, Asp106, Met108, Asn154, Tyr36	Hydrogen	Gly B:121, Tyr A:121	Hydrogen	Gly291, Thr292, Asp289, Trp137, Asn98, Arg189, Ile187, Phe169	Hydrogen	Phe B:250, Arg B:207, Ser A:63, Gly A:122, Ser B:205, Arg A:64
	Carbon Hydrogen	Thr110	Carbon Hydrogen	Leu D:157, Leu B:120, Tyr B:119, Ser B:60	Carbon Hydrogen	Gly95	Carbon Hydrogen	Ser B:249, Ser A:120
	Hydrophobic	Val A:39, Ile A:31, Leu:156, Ala A:52	Hydrophobic	Tyr A:119	Hydrophobic	Val393, Ile287, Ser96, Val130, Ser97, Tyr259, Tyr132, Ile179, Lys168, Trp176, Ile171, Leu91, Gln73, Gly74	Hydrophobic	Trp B:206, Ser B:251, Phe B:256, Ser A:65, Thr A:62, Tyr B:204, Cys A:163, Ala A:162, Gln A:161, Asn B:208, Lys B:210
Nigakilactone K	Hydrogen	Asp111, Tyr36	Hydrogen	-	Hydrogen	Trp137, Asp93	Hydrogen	Arg B:207, Thr A:62
	Carbon Hydrogen	Gln105, Thr110	Carbon Hydrogen	Ser D:60, Tyr D:151	Carbon Hydrogen	Gly95, Asp289, Gly291	Carbon Hydrogen	His A:121
	Hydrophobic	Ile103, Ala52, Ile53, Leu156, Cys166, Met108, Glu109, Ile, Lys114, Ser153, Gly32, Asn154, Glu33, Lys54, Asp167	Hydrophobic	Leu B:157, Tyr C:119, Tyr D:119, Tyr C:59, Leu C:120, Gly C:121, Gln D:61, Tyr D:59, Leu D:120, Gly D:121, Leu B:55, Leu D:57, Val D:123, Gly D:122, Ile D:58, Val B:123	Hydrophobic	Ser96, Tyr259, Ile287, Thr292, Leu91, Gly74, Gln73, Ile171, Lys168, Trp176, Phe169, Ile179, Thr133, Tyr132, Val130	Hydrophobic	Ser B:209, Ser A:65, Met A:61, Tyr B:204, Phe B:256, Cys A:163, Ser B:205, Trp B:206
Picrasin G	Hydrogen	Asp106, Met108	Hydrogen	Gly D:122	Hydrogen	-	Hydrogen	Cys A:163, Arg B:207
	Carbon Hydrogen	Asp167	Hydrophobic	Val D:123, Val B:123, Leu B:55, Leu B:157, Gly D:121, Tyr D:119, Ser D:60, Leu D:120, Tyr D:59, Tyr D:151, Leu C:120, Tyr C:59, Gly C:122, Leu C:57, Ile D:155, Leu D:57	Carbon Hydrogen	Gly291	Carbon Hydrogen	Ser B:206
	Hydrophobic	Glu71, Ala52, Leu156, Leu107, Lys114, Thr110, Glu109, Ile31, Asp111, Gly32, Tyr113, Glu33, Ser153, Tyr36, Asn154, Lys151, Cys166, Lys54		Hydrophobic	Thr133, Gln134, Lys168, Thr291, Asn294, Thr293, Gly72, Ile171, Gly74, Gln73, Trp176, Leu91, Ile179, Phe169, Tyr132, Ser96, Tyr132, Trp137	Hydrophobic	Ser B:209, Trp B:206, Arg A:64, Gln A:161, Ser A:120, His A:121, Ala A:162, Gly A:122, Thr A:62, Tyr B:204, Phe B:256	
Pterosin Y	Hydrogen	Lys54, Asp167, Gln105, Met108, Lys114, Asp111	Hydrogen	Gly C:121, Tyr C:151, Gln C:61	Hydrogen	Ser96, Ile187, Ser97, Arg189	Hydrogen	Arg B:207, Arg A:64
	Hydrophobic	Glu71, Tyr36, Asn154, Ser153, Leu157, Thr110, Glu109, Ile31, Leu107, Val39, Ile84, Ile53	Carbon Hydrogen	Ser C:60	Carbon Hydrogen	Asp93	Hydrophobic	Cys A:163, Trp B:206, Phe B:256, Gly A:122, Ala A:162, Ser B:213, Gln A:161
			Hydrophobic	Tyr C:59, Leu C:57, Ile C:58, Ile D:155, Leu D:57, Gly C:122, Tyr D:59, Ser D:60, Tyr D:151, Tyr D:119, Leu C:120, Tyr C:119	Hydrophobic	Leu91, Ile179, Gly181, Ala100, Trp137, Asn98, Ala188, Tyr259, Gly95, Val130, Tyr132, Phe169		

neuroinflammation (Sato et al., 2021). In the present study, several bioactive compounds identified from *C. sumatrana* ex-

hibited strong binding affinities toward BACE1, with some compounds demonstrating docking scores comparable to those of reference ligands. These findings suggest that the predicted neuroprotective potential of *C. sumatrana* may, at least in part, be mediated through modulation of the BACE1-associated amyloidogenic pathway, a mechanism that is highly relevant to currently approved anti-neurodegenerative therapies.

Although molecular docking provides valuable preliminary insight into the binding affinity and potential interactions between bioactive compounds of *C. sumatrana* and target proteins, the stability and dynamic behavior of these ligand–protein complexes under physiological conditions are more accurately evaluated through molecular dynamics (MD) simulations. MD simulations are important for validating docking results because they can assess conformational stability, interaction persistence, binding flexibility, and the overall reliability of the predicted complexes over time (Ramírez and Caballero, 2018). However, due to current limitations in computational facilities and resources, MD simulations could not be performed in the present study. Therefore, comprehensive MD simulation analysis should be considered a major priority for future investigations to further validate and strengthen the molecular interaction findings reported in this study. In addition, the potential inhibitory interactions between bioactive compounds from C. sumatrana extract and the MAPK1, BACE1, TNF-α, and CASP3 proteins were predicted solely through *in silico* simulations. Therefore, further validation using gene and protein expression analyses, such as qPCR and Western blotting, for MAPK1, BACE1, TNF-α, and CASP3 is necessary to confirm the proposed molecular mechanisms underlying their biological activities.

3.4 Antioxidant Capacity of *C. sumatrana* Extract

The antioxidant capacity of *C. sumatrana* extract was evaluated using DPPH, ABTS, and FRAP assays (Figure 6), revealing dose-dependent activity across all tests. In the DPPH assay, radical scavenging activity increased from 48.01% at 50 μg/mL to 78.05% at 500 μg/mL, with an IC_{50} of 52.6 μg/mL, indicating strong free radical neutralization potential. The ABTS assay showed lower scavenging activity, ranging from 3.05% at 25 μg/mL to 20.45% at 200 μg/mL, yielding a higher IC_{50} (497.7 μg/mL), suggesting reduced efficacy in this system. For the FRAP assay, the extract demonstrated moderate reducing power (RP), with RP_{50} of 195.2 μg/mL. These results collectively highlight the strongest antioxidant performance in the DPPH model, followed by FRAP and ABTS, aligning with its potential as a natural source of free radical scavengers, particularly effective at higher concentrations. The marked differences in IC_{50}/RP50 values across assays likely reflect variations in antioxidant mechanisms and sensitivity to the tested phytochemical constituents.

The *in vitro* antioxidant profile of ECS reveals a dose-dependent capacity to neutralize free radicals, though its efficacy varied significantly across assays (stronger in DPPH assay but weaker in FRAP and ABTS assays). Its strongest performance in the DPPH assay (IC_{50} 52.6 μg/mL) indicates superior hydrogen-donating ability-a property crucial for quenching lipid peroxidation cascades in neuronal membranes (Syukur et al., 2023; Durand et al., 2025). A strong DPPH scavenging activity of ECS likely attributes to the ability of bioactive compounds in the groups of flavonoids and terpenoids that serve as hydrogen donor to neutralize stable radicals. Otherwise, terpenoids, as major group found in *C. sumatrana*, is lacking of hydroxyl groups which are crucial for efficient electron or hydrogen transfer in neutralizing free radicals under FRAP and ABTS assays (Mohandas and Kumaraswamy, 2018). The potent DPPH scavenging is consistent with structure-activity relationships where hydroxylated flavonoids and terpenoids excel at radical stabilization (Sui et al., 2024) and may also contribute to chain-breaking antioxidant actions in lipid-rich environments like the brain tissue (Gutiérrez-Del-Río et al., 2021; Chen et al., 2025). The DPPH scavenging activity of ECS surpasses *C. aeruginosa* extract (DPPH IC_{50} 89.90 μg/mL) (Nurcholis et al., 2017) and *Zingiber zerumbet* extract (IC_{50} 100 μg/mL) (Assiry et al., 2023). However, it is lower than *C. longa* (IC_{50} 37.1 μg/mL) (Sabir et al., 2021), *C. aromatica* (IC_{50} 15.3 μg/mL) and *C. angusetifolia* extract (IC_{50} 16.08 μg/mL) (Albaqami et al., 2022) and curcumin from *C. zedoaria* (IC_{50} 44.06 μg/mL) (Shofia et al., 2024). The differences among species could be attributed to variations in their phytochemical constituents. Future comparative phytochemical profiling is needed to elucidate it.

The antioxidant activity observed in the present study should be interpreted as preliminary evidence based on chemical antioxidant assays. Among the assays performed, only the DPPH assay demonstrated strong antioxidant activity. While the results suggest that *C. sumatrana* possesses noticeable antioxidant potential, these assays do not fully reflect the complexity of antioxidant mechanisms in biological systems. Therefore, direct interpretation regarding intracellular oxidative stress modulation or cellular antioxidant effects cannot be drawn from the current findings alone. More comprehensive approaches, such as Oxygen Radical Absorbance Capacity (ORAC) analysis and cellular reactive oxygen species (ROS) assays, would provide stronger mechanistic evidence and greater biological relevance (Thanuma et al., 2025). However, these analyses were beyond the scope of the present study and could not be performed at this stage. Consequently, future studies should prioritize cellular and mechanistic antioxidant evaluations to validate the biological significance of the antioxidant activity observed and to further elucidate the underlying mechanisms of action of *C. sumatrana* extract.

It should also be akcnowledged that there is a discrepancy between moderate antioxidant activity of *C. sumatrana in vitro* and strong binding affinities of the compounds in the extract toward MAPK1, TNF-α, BACE1, and CASP3 *in silico*. This discrepancy may be attributed to the different mechanisms evaluated by these approaches. While DPPH, ABTS, and FRAP assays measure the direct radical-scavenging and reducing capacities of the extract (Rumpf et al., 2023), molecular docking predicts the ability of individual compounds to interact with

proteins involved in neuroinflammation, amyloidogenesis, and apoptosis. Nevertheless, these mechanisms are closely interconnected (Bi et al., 2025), as oxidative stress can activate inflammatory, amyloidogenic, and apoptotic pathways, whereas inhibition of these proteins may indirectly reduce oxidative damage and neuronal injury. Therefore, the neuroprotective potential of *C. sumatrana* may be mediated through a combination of moderate direct antioxidant activity and modulation of multiple molecular targets involved in neurodegenerative disease progression.

3.5 Anti-Neurodegenerative Activity of *C. sumatrana* Extract

The ECS significantly attenuated MSG-induced cognitive deficits across multiple behavioral paradigms (Figure 7). In the Hebbs-William Maze test, one-way ANOVA showed a significant difference in transfer latency among groups ($F(4,20) = 16.38$, $p < 0.0001$, $\eta^2 = 0.77$) (Figure 7A), indicating a very large treatment effect. The MSG group exhibited significantly higher transfer latency than the control group ($p < 0.0001$, Cohen's d = 3.11), whereas ECS at 75, 150, and 300 mg/kg BW significantly reduced latency compared with the MSG group ($p = 0.014$, 0.001, and < 0.0001; Cohen's d = 1.76, 2.84, and 3.89, respectively). No significant differences were observed between ECS 150 and 300 mg/kg BW ($p = 0.284$, Cohen's d = 0.88) or between the control and ECS 150 mg/kg BW groups ($p = 0.771$, Cohen's d = 0.42), indicating substantial cognitive recovery at higher doses.

Similarly, in the Morris Water Maze test, significant differences in escape latency were observed among groups ($F(4,20) = 12.94$, $p < 0.0001$, $\eta^2 = 0.72$) (Figure 7B). The MSG group showed significantly impaired spatial memory compared with the control group ($p = 0.001$, Cohen's d = 2.45). ECS at 150 and 300 mg/kg BW significantly reduced escape latency relative to the MSG group ($p = 0.018$ and < 0.0001; Cohen's d = 1.52 and 2.87, respectively). Notably, no significant difference was found between the control and ECS 300 mg/kg BW groups ($p = 0.964$, Cohen's d = 0.19), suggesting near-complete restoration of spatial memory performance.

In the hole-board test, one-way ANOVA also revealed significant differences in exploratory behavior ($F(4,20) = 7.86$, $p = 0.0006$, $\eta^2 = 0.61$) (Figure 7C). The MSG group displayed significantly reduced exploratory activity compared with the control group ($p = 0.003$, Cohen's d = 3.01), while ECS treatment at 75, 150, and 300 mg/kg BW significantly improved exploratory behavior ($p = 0.019$, 0.011, and 0.001; Cohen's d = 2.11, 1.79, and 2.84, respectively). No significant difference was observed between the control and ECS 300 mg/kg BW groups ($p = 0.638$, Cohen's d = 0.46). Overall, these findings demonstrate that ECS effectively ameliorated MSG-induced impairments in learning, memory, and exploratory behavior, with the 300 mg/kg BW dose showing the strongest neuroprotective effect.

In this present study, higher doses of ECS effectively normalized spatial learning, memory retrieval, and exploratory behavior. Similarly, a previous study also demonstrated that *C. zedoaria* extract could improve memory and learning in pentylenetetrazole-induced cognitive impairment in rats (Mahmoudi et al., 2020). Likewise, curcumin from *C. longa* is capable of preserving spatial memory in genetically engineered mouse model of Alzheimer's disease (Lamichhane et al., 2024), while a study by Kumar et al. (2023) indicated that curcumin could improve learning and memory in AlCl3-induced Alzheimer's rat model. The complete reversal of cognitive deficits at highest dose of ECS in our study mirrors effects seen with curcumin from *C. longa* in MSG-induced rats (Khalil and Khedr, 2016). Notably, the restoration of exploratory behavior, even at lower doses of ECS in our study, suggests early effects on motivational circuits, possibly via modulation of dopaminergic or glutamatergic systems-mechanisms previously implicated for terpenoids (Manayi et al., 2016), a major constituent of ECS.

Biochemical measurement revealed that MSG administration significantly elevated MDA levels in brain tissue, indicating increased lipid peroxidation. One-way ANOVA demonstrated a statistically significant difference in MDA levels among the experimental groups ($F(4,20) = 8.73$, $p = 0.0003$, $\eta^2 = 0.64$) (Figure 7D). ECS treatment attenuated this effect in a dose-dependent manner. Mice receiving the lowest ECS dose (75 mg/kg BW) showed no significant reduction in MDA levels ($p = 0.936$, Cohen's d = 0.18). However, higher ECS dose (300 mg/kg BW) significantly lowered MDA concentrations ($p = 0.039$, Cohen's d = 1.42). While the 300 mg/kg BW ECS group exhibited the strongest reduction, its MDA levels remained significantly higher than those of the control group ($p = 0.043$, Cohen's d = 1.62), suggesting partial but incomplete normalization of oxidative stress. These results demonstrate that higher ECS doses (300 mg/kg BW) effectively mitigate MSG-induced oxidative damage, with efficacy proportional to dosage.

MDA-a terminal product of polyunsaturated fatty acid oxidation-is a well-established marker of oxidative stress, elevated in Alzheimer's and Parkinson's patients(Sethiya et al., 2024). The dose-dependent MDA reduction directly correlates with the ECS *in vitro* antioxidant capacity, suggesting that its free radical scavenging activity translates to *in vivo* neuroprotection. This aligns with reports on curcumin of *C. longa* showing that its antioxidant properties mediate its anti-amyloidogenic effects ((Kleinrichert and Alappat, 2019).

The *C. sumatrana* extract (ECS) significantly mitigated MSG-induced histopathological damage in the hippocampal CA1 and CA3 regions of mice (Figures 8 and 9). Histopathological analysis revealed significant differences in hippocampal cell integrity among treatment groups. In the CA1 region, one-way ANOVA demonstrated a highly significant difference in degenerative cell counts ($F(4,20) = 41.82$, $p < 0.0001$, $\eta^2 = 0.89$) (Figure 9A), indicating a very large treatment effect. Bonferroni post hoc analysis showed significantly higher degenerative cell numbers in the MSG and ECS 75 mg/kg BW groups compared with the control group (both $p < 0.0001$; Cohen's d = 4.12 and

3.58, respectively). In contrast, ECS 150 and 300 mg/kg BW significantly reduced degenerative cell counts compared with the MSG group (p = 0.002 and 0.001; Cohen's d = 2.74 and 2.81, respectively), with no significant difference between ECS 150 and 300 mg/kg BW (p = 0.991, Cohen's d = 0.09). Similarly, in the CA3 region, one-way ANOVA revealed significant differences in degenerative cell counts ($F(4,20) = 37.56$, $p < 0.0001$, $\eta^2 = 0.88$) (Figure 9C). Bonferroni analysis indicated significantly increased degeneration in the MSG and ECS 75 mg/kg BW groups compared with the control group (both $p < 0.0001$; Cohen's d = 3.76 and 3.41, respectively), whereas ECS 150 and 300 mg/kg BW significantly reduced degeneration relative to the MSG group (p = 0.001 and 0.002; Cohen's d = 2.63 and 2.49, respectively). No significant difference was observed between ECS 150 and 300 mg/kg BW (p = 0.873, Cohen's d = 0.18).

For viable cells, no significant difference was detected in the CA1 region ($F(4,20) = 2.11$, $p = 0.118$, $\eta^2 = 0.29$), and all pairwise comparisons were non-significant ($p > 0.05$) (Figure 9B). However, significant differences were observed in viable cell counts within the CA3 region ($F(4,20) = 8.94$, $p = 0.0003$, $\eta^2 = 0.64$) (Figure 9D). Bonferroni analysis demonstrated that the MSG group had significantly fewer viable cells than the control, ECS 75 mg/kg BW, ECS 150 mg/kg BW, and ECS 300 mg/kg BW groups (p = 0.004, 0.011, 0.015, and 0.009; Cohen's d = 1.92, 1.44, 1.38, and 1.51, respectively), whereas no significant differences were found among the ECS-treated groups ($p > 0.05$). Overall, these findings indicate that ECS treatment effectively reduced hippocampal neurodegeneration and preserved neuronal viability, particularly in the CA3 region.

Histopathological examination provided supportive evidence that *C. sumatrana* protected the hippocampus from MSG-induced neuronal damage. As a brain region that plays a central role in learning and memory, the hippocampus is highly vulnerable to oxidative stress and excitotoxic injury, making it one of the most affected areas in neurodegenerative disorders such as Alzheimer's disease (Pluta et al., 2021). In the present study, ECS at higher doses significantly reduced neuronal degeneration in both the CA1 and CA3 regions, whereas the lower dose was insufficient to produce a comparable protective effect. Interestingly, increasing the dose of ECS from 150 to 300 mg/kg BW did not result in additional protection, suggesting that the optimal neuroprotective effect may already have been achieved at 150 mg/kg BW. The preservation of viable neurons, particularly in the CA3 region, further highlights the ability of ECS to maintain hippocampal integrity under neurotoxic conditions. The CA3 region appeared to respond more favorably to treatment, as reflected by the greater preservation of non-degenerated neurons. This finding may be related to differences in the expression of neuroprotective factors, such as Brain-Derived Neurotrophic Factor (BDNF) and Nerve Growth Factor (NGF), which play important roles in neuronal survival and synaptic plasticity (Wihadmadyatami et al., 2025). Consistent with the present findings, *C. longa* and its major bioactive compound, curcumin, have been reported to protect neurons in the hippocampal CA1 and CA3 regions and improve brain health in experimental models (Banji et al., 2021; González-Granillo et al., 2022).

The neuroprotective effects of *C. sumatrana* are likely attributable to the diverse bioactive compounds present in the extract. It is speculated that these compounds exert their beneficial effects through several mechanisms, including reducing oxidative stress, suppressing inflammatory signaling pathways (such as TNF-α and MAPK), and inhibiting apoptosis. This is particularly important because oxidative stress, neuroinflammation, and apoptosis are recognized as key contributors to hippocampal degeneration and the progression of neurodegenerative diseases (Dash et al., 2025). Therefore, targeting these pathological processes is crucial for maintaining neuronal health and slowing disease progression (Adamu et al., 2024; Altahrawi et al., 2025).

The phytochemical constituents identified in the extract may exhibit both synergistic and antagonistic interactions that collectively influence their potential neuroprotective activity against neurodegenerative diseases. Several compounds, particularly Genistein, Artemisic acid, Furanodiene, and 8-Epiloganic acid-6'-O-beta-D-glucoside, may act synergistically through complementary mechanisms involving antioxidant, anti-inflammatory, and anti-apoptotic pathways. Genistein is widely associated with suppression of TNF-α, NF-κB, and MAPK signaling (Khairudin et al., 2025), while sesquiterpenoid compounds such as artemisic acid and furanodiene may contribute to the reduction of oxidative stress, mitochondrial dysfunction, and neuronal apoptosis (Yan et al., 2021). In addition, iridoid glycosides such as 8-epi-loganic acid-6'-O-beta-D-glucoside may enhance cellular resilience and neuroprotective signaling. Alkaloid compounds such as Fawcettimine may further support neurotransmission and neuronal survival, potentially enhancing cognitive protection through cholinergic modulation. Moreover, sesquiterpenoids including Alpha-khusinol and Linderazulene may synergistically stabilize neuronal membranes and attenuate lipid peroxidation. Quassinoid compounds such as Nigakilactone K and Picrasin G may also cooperatively regulate inflammatory and apoptotic signaling pathways associated with MAPK1, TNFα, and CASP3 modulation. However, potential antagonistic interactions may also occur. Brefeldin A, despite possessing certain bioactivities, is known to induce Golgi and endoplasmic reticulum stress (Oh-Hashi et al., 2021), which at higher concentrations may enhance neuronal apoptosis and counteract neuroprotective effects. Competition among lipophilic terpenoid compounds for metabolic enzymes, plasma protein binding, or blood–brain barrier transport may additionally alter compound bioavailability and pharmacological effectiveness. Therefore, the neuroprotective activity of the extract is likely mediated by a complex polypharmacological interaction network involving both synergistic and antagonistic mechanisms among its phytochemical constituents.

4. CONCLUSIONS

This study demonstrated the neuroprotective potential of *C. sumatrana* through phytochemical, computational, *in vitro*, and *in vivo* analyses. LC-MS/MS-QTOF profiling identified 13 compounds, predominantly terpenoids. *In silico* analyses predicted antioxidant, anti-inflammatory, and antineurodegenerative activities, while drug-likeness assessment suggested favorable bioavailability for all identified compounds. ADMET prediction highlighted artemisic acid, genistein, picrasin G, brefeldin A, and α-khusinol as the promising pharmacokinetic candidates, whereas dendronobilin F exhibited the lowest predicted toxicity. Furthermore, molecular docking targeting neurodegeneration-associated proteins revealed strong interactions of brefeldin A, nigakilactone K, genistein, and 8-epi-loganic acid-6'-O-β-D-glucoside with MAPK1, TNF-α, BACE1, and CASP3, respectively. In addition, the rhizome extract exhibited antioxidant activity, particularly in the DPPH assay, and significantly ameliorated MSG-induced cognitive impairment, hippocampal neurodegeneration, and elevation of brain MDA levels in mice. Collectively, these findings suggest that *C. sumatrana* is a promising source of neuroprotective agents, plausibly acting through the modulation of neurodegeneration-related pathways and antioxidant mechanisms. Further studies are needed to isolate the active compounds and validate their therapeutic efficacy and molecular mechanisms.

5. ACKNOWLEDGEMENT

This study was funded by the PUJK Grant (Penelitian Unggulan Jalur Kepakaran) of LPPM Universitas Andalas (Contract No. 397/UN16.19/PT.01.03/PUJK/2025; P Santoso as principal researcher). The authors thank Prof. Dr. Marzuki (Head of LPPM Universitas Andalas) for facilitating this grant.

REFERENCES

Adamu, A., S. Li, F. Gao, and G. Xue (2024). The Role of Neuroinflammation in Neurodegenerative Diseases: Current Understanding and Future Therapeutic Targets. *Frontiers in Aging Neuroscience*, **16**; 1347987

Alam, A., M. A. Hosen, A. Hosen, Y. Fujii, Y. Ozeki, and S. M. Abe Kawsar (2021). Synthesis, Characterization, and Molecular Docking Against a Receptor Protein FimH of *Escherichia coli* (4XO8) of Thymidine Derivatives. *Journal of the Mexican Chemical Society*, **65**(2); 256–276

Alamsjah, F., A. Agustien, and T. Alam (2023). Antibacterial Activity of *Curcuma sumatrana* Miq. Rhizome Extract, an Endemic Plant of West Sumatra, Against Gram-Positive Bacteria. *Bioscientist Journal*, **9**(1); 63–71

Albaqami, J. J., H. Hamdi, A. Narayanankutty, N. U. Visakh, A. Sasidharan, A. M. Kuttithodi, A. C. Famurewa, and B. Pathrose (2022). Chemical Composition and Biological Activities of the Leaf Essential Oils of *Curcuma longa*, *Curcuma aromatica*, and *Curcuma angustifolia*. *Antibiotics*, **11**(11); 1547

Altahrawi, A. Y., A. W. James, and Z. A. Shah (2025). The Role of Oxidative Stress and Inflammation in the Pathogenesis and Treatment of Vascular Dementia. *Cells*, **14**(8); 609

Andronie-Cioara, F. L., A. I. Ardelean, C. D. Nistor-Cseppento, A. Jurcau, M. C. Jurcau, N. Pascalau, and F. Marcu (2023). Molecular Mechanisms of Neuroinflammation in Aging and Alzheimer's Disease Progression. *International Journal of Molecular Sciences*, **24**(3); 1869

Arafat, M. T., H. R. Ghaiad, and E. M. Elbaz (2025). Genistein Exerts Neuroprotective Effects in an Ouabain-Induced Model of Bipolar Disorder: Behavioral and Molecular Insights. *Neurochemical Research*, **51**(1); 10

Assiry, A. A., N. Ahmed, A. Almuaddi, A. Saif, M. A. Alshahrani, R. N. Mohamed, and M. I. Karobari (2023). The Antioxidant Activity, Preliminary Phytochemical Screening of *Zingiber zerumbet* and Antimicrobial Efficacy Against Selective Endodontic Bacteria. *Food Science & Nutrition*, **11**(8); 4853–4860

Banji, D., O. J. F. Banji, and K. Srinivas (2021). Neuroprotective Effect of Turmeric Extract in Combination with Its Essential Oil and Enhanced Brain Bioavailability in an Animal Model. *BioMed Research International*, **2021**; 6645720

Bartolić, M. and A. Bosak (2025). BACE1: Biological Functions and Involvement in the Pathophysiology of Alzheimer's Disease and Other Neurological Disorders. *BioFactors*, **51**(6); e70071

Bi, D., H. Bao, X. Yang, Z. Wu, X. Yang, G. Xu, X. Liu, Z. Wan, J. Liu, J. He, L. Wen, Y. Jing, R. Zhu, Z. Long, Y. Rong, D. Wang, X. Wang, W. Xiong, G. Huang, F. Gao, and Y. Shen (2025). BACE1-Dependent Cleavage of GABAA Receptor Contributes to Neural Hyperexcitability and Disease Progression in Alzheimer's Disease. *Neuron*, **113**(7); 1051–1064.e6

Chen, C., W. Dai, L. Zhang, D. Wang, X. Jiang, and M. Zhang (2022). Antioxidant Effects of Diarylheptanoids from Two *Curcuma* Species. *Natural Product Research*, **36**(22); 5732–5739

Chen, Q., G. Chen, and Q. Wang (2025). Application of Network Pharmacology in the Treatment of Neurodegenerative Diseases with Traditional Chinese Medicine. *Planta Medica*, **91**(5); 226–237

Chen, X., H. Li, L. Tian, Q. Li, J. Luo, and Y. Zhang (2020). Analysis of the Physicochemical Properties of Acaricides Based on Lipinski's Rule of Five. *Journal of Computational Biology*, **27**(9); 1397–1406

Dai, W., D. Wang, C. Chen, and M. Zhang (2023). Antioxidation Abilities of Sesquiterpenoids from *Curcuma aromatica* in Vitro. *Combinatorial Chemistry & High Throughput Screening*, **26**(1); 236–240

Dash, U. C., N. K. Bhol, S. K. Swain, R. R. Samal, P. K. Nayak, V. Raina, S. K. Panda, R. G. Kerry, A. K. Duttaroy, and A. B. Jena (2025). Oxidative Stress and Inflammation in the Pathogenesis of Neurological Disorders: Mechanisms and Implications. *Acta Pharmaceutica Sinica B*, **15**(1); 15–34

Divyashri, G., T. P. Krishna Murthy, S. Sundareshan, P. Ka-

math, M. Murahari, G. R. Saraswathy, and B. Sadanandan (2021). In Silico Approach Towards the Identification of Potential Inhibitors from *Curcuma amada* Roxb Against *H. pylori*: ADMET Screening and Molecular Docking Studies. *BioImpacts*, **11**(2); 119–127

Durand, E., M. Laguerre, C. Bourlieu-Lacanal, J. Lecomte, and P. Villeneuve (2025). Navigating the Complexity of Lipid Oxidation and Antioxidation: A Review of Evaluation Methods and Emerging Approaches. *Progress in Lipid Research*, **97**; 101317

Elhawary, E. A., A. Y. Moussa, and A. N. B. Singab (2024). Genus *Curcuma*: Chemical and Ethnopharmacological Role in Aging Process. *BMC Complementary Medicine and Therapies*, **24**(1); 31

Essawy, A. E., E. M. Jimmiey, W. M. Abdel-Wahab, R. G. Ali, S. M. Eweda, and H. M. Abdou (2025). The Protective Efficacy of Omega-3 Polyunsaturated Fatty Acids on Oxidative Stress, Inflammation, Neurotransmitter Perturbations, and Apoptosis Induced by Monosodium Glutamate in the Brain of Male Rats. *Metabolic Brain Disease*, **40**(1); 114

Fan, F., H. Liu, X. Shi, Y. Ai, Q. Liu, and Y. Cheng (2022). The Efficacy and Safety of Alzheimer's Disease Therapies: An Updated Umbrella Review. *Journal of Alzheimer's Disease*, **85**(3); 1195–1204

Gabr, M. T. and M. S. Abdel-Raziq (2018). Design and Synthesis of Donepezil Analogues as Dual AChE and BACE-1 Inhibitors. *Bioorganic Chemistry*, **80**; 245–252

Genchi, G., G. Lauria, A. Catalano, A. Carocci, and M. S. Sinicropi (2024). Neuroprotective Effects of Curcumin in Neurodegenerative Diseases. *Foods*, **13**(11); 1774

González-Granillo, A. E., D. Gnecco, A. Díaz, L. Garcés-Ramírez, F. de la Cruz, I. Juarez, J. C. Morales-Medina, and G. Flores (2022). Curcumin Induces Cortico-Hippocampal Neuronal Reshaping and Memory Improvements in Aged Mice. *Journal of Chemical Neuroanatomy*, **121**; 102091

Gutiérrez-Del-Río, I., S. López-Ibáñez, P. Magadán-Corpas, L. Fernández-Calleja, Á. Pérez-Valero, M. Tuñón-Granda, E. M. Miguélez, C. J. Villar, and F. Lombó (2021). Terpenoids and Polyphenols as Natural Antioxidant Agents in Food Preservation. *Antioxidants*, **10**(8); 1264

Han, Q., J. Zhu, and P. Zhang (2023). Mechanisms of Main Components in *Curcuma longa* L. on Hepatic Fibrosis Based on Network Pharmacology and Molecular Docking: A Review. *Medicine*, **102**(29); e34353

Hasballah, K., M. Murniana, M. Marlina, B. Bakhtiar, D. K. Rusly, B. Ginting, T. Maidiani, S. Rahmazani, and D. D. Rampengan (2026). DPPH and Hep2 Cell Inhibitions by Ethyl Acetate Extract and Its Fractions from Indonesian *Cassia siamea* L. Stem Barks: In Vitro and Computational Prediction. *Science and Technology Indonesia*, **11**(1); 235–251

Hussen, E. M. and S. A. Endalew (2023). In Vitro Antioxidant and Free-Radical Scavenging Activities of Polar Leaf Extracts of *Vernonia amygdalina*. *BMC Complementary Medicine and Therapies*, **23**(1); 146

Jeon, M. T., S. A. Cogill, K. S. Kim, Y. Kim, H. Kim, C. Y. Lee, S. Kim, S. Son, J. Kim, J. Lee, I. Park, M. Cheon, and D. G. Kim (2025). TNF-α-NF-κB Activation Through Pathological α-Synuclein Disrupts the BBB and Exacerbates Axonopathy. *Cell Reports*, **44**(7); 116001

John, E., B. Mishra, A. S. Tripathi, and R. Aleesha (2022). Protective Effect of *Celastrus paniculatus* on Cognitive Function in Glutamate-Induced Brain-Injured Mice by Reducing Intracellular Calcium Influx. *International Journal of Developmental Neuroscience*, **82**(4); 331–338

Kh, A. E. A. K., S. Qadeer, S. A. Gabr, A. M. Shehabeldin, A. E. B. Ghodaia, S. Latif, and A. U. Husna (2025). Molecular Docking of Nano-Curcumin to Caspase-3 and Caspase-9: Unraveling Its Cryoprotective Mechanism in Rabbit Sperm Extenders. *Reproductive Biology*, **25**(4); 101071

Khairudin, N. Y. M., A. Mohd Azraai, R. Siran, and N. Azme (2025). Therapeutic Mechanisms of Genistein in Ischemic Stroke: A Systematic Review of In Vivo and In Vitro Studies. *PLoS One*, **20**(12); e0338590

Khalil, R. M. and N. F. Khedr (2016). Curcumin Protects Against Monosodium Glutamate Neurotoxicity and Decreases NMDA2B and mGluR5 Expression in Rat Hippocampus. *Neuro-Signals*, **24**; 81–87

Kleinrichert, K. and B. Alappat (2019). Comparative Analysis of Antioxidant and Anti-Amyloidogenic Properties of Various Polyphenol-Rich Phytoceutical Extracts. *Antioxidants*, **8**(1); 13

Kumar, P., A. Singh, A. Kumar, R. Kumar, R. Pal, A. K. Sachan, R. K. Dixit, and R. Nath (2023). Effect of Curcumin and Coenzyme Q10 Alone and in Combination on Learning and Memory in an Animal Model of Alzheimer's Disease. *Biomedicines*, **11**(5); 1422

Lamichhane, G., J. Liu, S. J. Lee, D. Y. Lee, G. Zhang, and Y. Kim (2024). Curcumin Mitigates High-Fat High-Sugar Diet-Induced Impairment of Spatial Memory, Hepatic Metabolism, and Gut Microbiome Alteration in Alzheimer's Disease Mice. *Nutrients*, **16**(2); 240

Mahmoudi, T., Z. Lorigooini, M. Rafieian-Kopaei, M. Arabi, Z. Rabiei, E. Bijad, and S. Kazemi (2020). Effect of *Curcuma zedoaria* Hydro-Alcoholic Extract on Learning, Memory Deficits, and Oxidative Damage Following Induced Seizures. *Behavioral and Brain Functions*, **16**(1); 7

Manayi, A., S. M. Nabavi, M. Daglia, and S. Jafari (2016). Natural Terpenoids as a Promising Source for Modulation of GABAergic System and Treatment of Neurological Diseases. *Pharmacological Reports*, **68**(4); 671–679

Mehla, J., P. Gupta, M. Pahuja, D. Diwan, and D. Diksha (2020). Indian Medicinal Herbs and Formulations for Alzheimer's Disease: from Traditional Knowledge to Scientific Assessment. *Brain Sciences*, **10**(12); 964

Mishra, R. and A. Upadhyay (2025). An Update on Mammalian and Non-Mammalian Animal Models for Biomarker Development in Neurodegenerative Disorders. *Cellular and Molecular Life Sciences*, **82**(1); 147

Mohandas, G. G. and M. Kumaraswamy (2018). Antioxidant Activities of Terpenoids from *Thuidium tamariscellum*. *Phar-*

macognosy Journal, **10**(4); 645–649
Nurcholis, W., N. Khumaida, M. Syukur, and M. Bintang (2017). Evaluation of Free Radical Scavenging Activity in Ethanolic Extract from *Curcuma aeruginosa* Roxb. *Molekul*, **12**(2); 133–138
Oh, K. N., D. R. Oh, Y. Kim, and S. Kim (2025). Protective Effects of *Curcuma longa* on Corticosterone-Induced Neurotoxicity and Depression-Like Behavior. *Journal of Microbiology and Biotechnology*, **35**; e2506005
Oh-Hashi, K., T. Hasegawa, Y. Mizutani, K. Takahashi, and Y. Hirata (2021). Elucidation of Brefeldin A-Induced ER and Golgi Stress Responses in Neuro2a Cells. *Molecular and Cellular Biochemistry*, **476**(10); 3869–3877
Oliveira, M. T. A., M. V. O. B. de Alencar, V. P. A. Landim, G. M. M. Moura, J. I. O. da Cruz, E. A. dos Santos, H. D. M. Coutinho, J. C. Andrade, I. R. A. de Menezes, P. R. V. Ribeiro, E. S. de Brito, E. O. de Sousa, and A. F. Uchoa (2020). UPLC-MS-QTOF Analysis and Antifungal Activity of Cumaru (*Amburana cearensis*). *3 Biotech*, **10**(12); 545
Passeri, E., K. Elkhoury, M. Morsink, K. Broersen, M. Linder, A. Tamayol, C. Malaplate, F. T. Yen, and E. Arab-Tehrany (2022). Alzheimer's Disease: Treatment Strategies and Their Limitations. *International Journal of Molecular Sciences*, **23**(22); 13954
Perez, A., H. A. Martinez-Correa, F. Parada-Alfonso, Z. J. Suárez Montenegro, D. Ballesteros-Vivas, G. Álvarez-Rivera, A. Cifuentes, and E. Ibáñez (2025). Antioxidant, Neuroprotective and Anti-Inflammatory Activity of *Curcuma longa* Extracts: From Green Extraction to Nanoemulsion. *Frontiers in Nutrition*, **12**; 1619725
Petrovsky, I., P. Santoso, and M. S. Fadil (2026). In Silico Insights into Bioactive Compounds of Wild Sumatran Turmeric (*Curcuma sumatrana*, Zingiberaceae) as Potent Antioxidant Candidates. *Al-Kauniyah: Jurnal Biologi*, **19**(1); 163–176
Pluta, R., L. Ouyang, S. Januszewski, Y. Li, and S. J. Czuczwar (2021). Participation of Amyloid and Tau Protein in Post-Ischemic Neurodegeneration of the Hippocampus. *International Journal of Molecular Sciences*, **22**(5); 2460
Pomalango, Z. B., M. A. Paneo, N. Pakaya, L. O. Aman, and A. H. Hutuba (2025). Cholesterol-Lowering Effects of Turmeric Effervescent Dosage in Preventing Atherosclerosis. *Science and Technology Indonesia*, **10**(2); 482–492
Qi, Y., J. Zhang, Y. Zhang, H. Zhu, J. Wang, X. Xu, S. Jin, C. Wang, F. Zhang, M. Zhao, Z. Wu, H. Zhu, and P. Yan (2025). *Curcuma wenyujin* Extract Alleviates Cognitive Deficits and Restrains Pyroptosis Through PINK1/Parkin-Mediated Autophagy. *Phytomedicine*, **139**; 156482
Rahman, A. T., A. Jethro, P. Santoso, V. D. Kharisma, and A. A. Murtadlo (2022). In Silico Study of Endemic Sumatra Wild Turmeric (*Curcuma sumatrana*) as Anti-Cancer. *Pharmacognosy Journal*, **14**(6); 806–812
Ramírez, D. and J. Caballero (2018). Reliability of Molecular Docking Scoring without Structural Validation. *Molecules*, **23**(5); 1038
Rumpf, J., R. Burger, and M. Schulze (2023). Statistical Evaluation of DPPH, ABTS, FRAP, and Folin-Ciocalteu Assays to Assess the Antioxidant Capacity of Lignins. *International Journal of Biological Macromolecules*, **233**; 123470
Sabir, S. M., A. Zeb, M. Mahmood, S. R. Abbas, Z. Ahmad, and N. Iqbal (2021). Phytochemical Analysis and Biological Activities of Ethanolic Extract of *Curcuma longa* Rhizome. *Brazilian Journal of Biology*, **81**(3); 737–740
Santoso, P., S. Ilyas, Y. H. Midoen, R. Maliza, and D. F. Belahusna (2024). Predictive Bioactivity of *Vitis gracilis* Leaf Extract Against Doxorubicin-Induced Cardiotoxicity. *Journal of Applied Pharmaceutical Science*, **14**(4); 99–114
Santoso, P., A. S. Simatupang, A. Fajria, R. Rahayu, and R. Jannatan (2023). Andaliman (*Zanthoxylum acanthopodium*) Extract Attenuates Hyperglycemia and Neurological Dysfunction. *Journal of Advanced Veterinary and Animal Research*, **10**(4); 608–619
Sarkar, B., N. Rana, C. Singh, and A. Singh (2024). Medicinal Herbal Remedies in Neurodegenerative Diseases: Antioxidant Potential Update. *Naunyn-Schmiedeberg's Archives of Pharmacology*, **397**(8); 5483–5511
Satir, T. M., L. Agholme, A. Karlsson, M. Karlsson, P. Karila, S. Illes, P. Bergström, and H. Zetterberg (2020). Partial Reduction of Amyloid β Production by β-Secretase Inhibitors Does Not Decrease Synaptic Transmission. *Alzheimer's Research & Therapy*, **12**(1); 63
Sato, K., T. Mano, A. Iwata, and T. Toda (2021). Safety of Memantine in Combination with Potentially Interactive Drugs in the Real World: A Pharmacovigilance Study Using the Japanese Adverse Drug Event Report (JADER) Database. *Journal of Alzheimer's Disease*, **82**(3); 1333–1344
Senobari, Z. S., H. M. Masoumian, M. B. Teimouri, A. H. Rezayan, S. Samarghandian, and A. Hekmat (2023). Chromone-Based Inhibitors Against SARS-CoV-2: Docking and MD Simulation Study. *BMC Research Notes*, **16**(1); 224
Sethiya, N. K., N. Ghiloria, A. Srivastav, D. Bisht, S. K. Chaudhary, V. Walia, and M. S. Alam (2024). Therapeutic Potential of Myricetin in Neurological Disorders. *CNS & Neurological Disorders - Drug Targets*, **23**(7); 865–882
Shahrajabian, M. H. and W. Sun (2024). Turmeric and Curcuminoids: Pharmacological Benefits. *Current Organic Synthesis*, **21**(5); 665–683
Shakira and M. Maulina (2025). Exploration of *Moringa oleifera* and *Curcuma longa* Compounds as Multi-Target Agents for Alzheimer's Disease. *Scripta Score Scientific Medical Journal*, **7**(1); 26–35
Shi, J., Y. E. Kim, N. J. DeRuiter, P. Kadav, and M. Tessier-Lavigne (2026). Caspase-3 Cleaves and Activates the NADase SARM1 to Promote Apoptosis, Linking Two Cell Death Mechanisms. *Proceedings of the National Academy of Sciences of the United States of America*, **123**(4); e2528118123
Shofia, V., A. B. Anggraeni, and H. Nurlaila (2024). Antioxidant Activity of Curcumin Extract from *Curcuma zedoaria* and *Curcuma longa*. *Indonesian Journal of Science and Pharmacy*,

1(3); 108–112
Shrestha, A., R. Marahatha, S. Basnet, B. P. Regmi, S. Katuwal, S. R. Dahal, K. R. Sharma, A. Adhikari, R. C. Basnyat, and N. Parajuli (2022). Flavonoids as SARS-CoV-2 Inhibitors: Docking and Dynamics Simulation. *Advances in Pharmacological and Pharmaceutical Sciences*, **2022**; 3742318
Singh, A., U. Soni, P. K. Varadwaj, K. Misra, and S. I. Rizvi (2025). Anti-Inflammatory Effect of Curcumin in Accelerated Senescence Model. *Journal of Biomolecular Structure and Dynamics*, **43**(3); 1459–1470
Söderberg, L., M. Johannesson, P. Nygren, H. Laudon, F. Eriksson, G. Osswald, C. Möller, and L. Lannfelt (2023). Lecanemab, Aducanumab, and Gantenerumab—Binding Profiles to Different Forms of Amyloid-Beta Might Explain Efficacy and Side Effects in Clinical Trials for Alzheimer's Disease. *Neurotherapeutics*, **20**(1); 195–206
Sohrab, S., P. Mishra, V. Dwivedi, P. Veis, A. K. Pathak, and S. K. Mishra (2024). Elemental and Metabolic Profiling of Zingiberaceae Using FT-IR and LIBS. *Heliyon*, **10**(13); e33395
Spiegel, M., K. Kapusta, W. Kołodziejczyk, J. Saloni, B. Żbikowska, G. A. Hill, and Z. Sroka (2020). Antioxidant Activity of Phenolic Acids and QSAR Analysis. *Molecules*, **25**(13); 3088
Sudhishma, S., S. D. Acharya, S. D. Ullal, V. Blossom, A. Parida, and N. Noushida (2021). Levetiracetam Exposure Induces Cognitive Decline Not Fully Prevented by *Bacopa monnieri*. *Journal of Complementary and Integrative Medicine*, **19**(4); 897–903
Sui, X., J. Wang, Z. Zhao, B. Liu, M. Liu, M. Liu, C. Shi, X. Feng, Y. Fu, D. Shi, S. Li, Q. Qi, M. Xian, and G. Zhao (2024). Phenolic Compounds Induce Ferroptosis-Like Death via Hydroxyl Radical Generation. *Communications Biology*, **7**(1); 199
Syafira, F., Nurainas, and Syamsuardi (2024). New Record and Spatial Distribution of *Curcuma sumatrana* in Sumatra. *Biodiversitas*, **25**; 4127–4138
Syukur, M., M. S. Prahasiwi, Nurkhasanah, S. Yuliani, Y. Purwaningsih, and E. Indriyanti (2023). Profiling of Active Compounds of Ethanol Extract, n-Hexane Extract, Ethyl Acetate Extract and Ethanol Fraction of Star Anise (*Illicium verum* Hook. f.) and Determination of Total Flavonoids, Total Phenolics and Their Potential as Antioxidants. *Science and Technology Indonesia*, **8**(2); 219–226
Thanuma, J., J. Phetcharaburanin, H. Dokduang, W. Loilome, P. Klanrit, A. Wangwiwatsin, and N. Namwat (2025). Metabolomic Analysis of Bioactive Compounds in Dill (*Anethum graveolens* L.) Extracts. *PeerJ*, **13**; e19567
Wang, S., Y. Jiang, A. Yang, F. Meng, and J. Zhang (2024). Expanding Burden of Neurodegenerative Diseases. *Aging and Disease*
Wang, Y., H. Zhang, J. Wang, M. Yu, Q. Zhang, S. Yan, D. You, L. Shi, L. Zhang, L. Wang, H. Wu, and X. Cao (2021). *Aconiti lateralis* Radix Praeparata Inhibits Alzheimer's Disease via GRIN1 and MAPK1. *Pharmaceutical Biology*, **59**(1); 311–320
Wihadmadyatami, H., M. A. Zulfikar, H. Herawati, S. Karnati, G. R. Saragih, D. Aliffia, D. A. O. A. Pratama, N. Handayani, U. Kustiati, D. R. Tirtosari, and Y. Tjahjono (2025). Neuroprotection of Stem Cell-Conditioned Medium in Alzheimer's Disease Model. *Open Veterinary Journal*, **15**(1); 151–161
Wójcik, P., M. K. Jastrzębski, A. Zięba, D. Matosiuk, and A. A. Kaczor (2024). Caspases in Alzheimer's Disease: Activation and Therapeutic Potential. *Molecular Neurobiology*, **61**(7); 4834–4853
Wu, H., Z. Liu, Y. Zhang, B. Gao, Y. Li, X. He, J. Sun, U. Choe, P. Chen, R. A. Blaustein, and L. Yu (2024). Chemical Composition and Antioxidant Activity of Turmeric Ethanol Extract. *Foods*, **13**(10); 1550
Wu, X., Z. Yang, J. Zou, H. Gao, Z. Shao, C. Li, and P. Lei (2025). Protein Kinases in Neurodegenerative Diseases: Current Understandings and Implications for Drug Discovery. *Signal Transduction and Targeted Therapy*, **10**(1); 146
Yan, J., H. Ma, X. Lai, J. Wu, A. Liu, J. Huang, W. Sun, M. Shen, and Y. Zhang (2021). Artemisinin Attenuated Oxidative Stress and Apoptosis by Inhibiting Autophagy in MPP^+-Treated SH-SY5Y Cells. *Journal of Biological Research (Thessaloniki)*, **28**(1); 6
Yuhendri, R., Nurainas, T. Maideliza, L. Meriko, Alponsin, and I. R. A. Wahab (2024). Anatomy and Powder Microscopy of *Curcuma sumatrana*. *Biodiversitas*, **25**; 900–908
Zhang, Q., Y. Xu, Y. Sun, H. Dong, D. Sun, H. Li, and L. Chen (2024). Terpenoids from *Curcuma kwangsiensis* and Their Anti-Inflammatory Activities. *Fitoterapia*, **178**; 106137
Zhang, X., J. Xu, Y. Fan, G. Shi, B. Chen, A. Wang, Y. Zhu, L. Li, H. Jia, D. Gheyret, J. Wang, Y. Cao, S. Li, X. Chen, J. Zhang, and S. Zhang (2025). Neutrophil Extracellular Traps Aggravate Neuronal Apoptosis After Traumatic Brain Injury. *Theranostics*, **15**(15); 7327–7345

